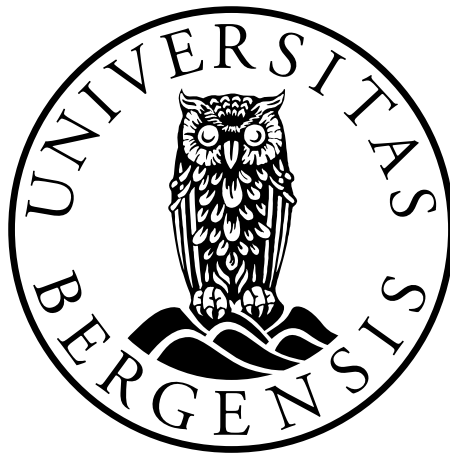


# The Effect of Electroconvulsive Therapy and Transcranial Magnetic Stimulation on Brain Volumes and Perfusion in Depression

**Ingrid Kleive Andersen**

Master's Thesis in Medical Technology



Department of Physics and Technology

University of Bergen

June 2024



# Abstract

Major depressive disorder is a common mental disorder and is characterized by experiencing a depressed mood and thoughts of hopelessness or suicide [1]. Bipolar disorder is a mental illness that causes changes in a person's mood, energy, and activity levels [2]. Electroconvulsive Therapy (ECT) and Transcranial Magnetic Stimulation (TMS) are treatment options for treatment-resistant depression [3][4] and bipolar disorder [2]. Volume changes in areas like the hippocampus are common findings in ECT studies [5]. There are fewer studies of volume change after TMS, but volume changes in the hippocampus have been found [6]. Studies on brain perfusion, or Cerebral Blood Flow (CBF), after ECT are sparse and primarily focus on how perfusion correlates with clinical outcome [7].

This study aimed to investigate if there is a connection between changes in brain perfusion and volume changes in areas of the brain. The hypothesis is that the ECT and TMS treatment will increase volume in specific brain regions and that these areas will experience a change in perfusion.

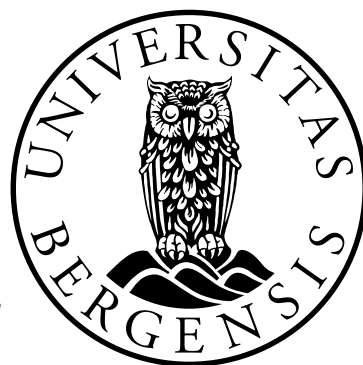
FreeSurfer [8] and FSL BASIL [9] were used to analyze the images. FreeSurfer was used for image segmentation and volume quantification, while FreeSurfer and FSL BASIL were used for perfusion quantification. A pipeline was established to analyze the data, and statistical analyses were performed to find statistically significant changes.

The results showed a statistically significant volumetric increase in the left (2.8%,  $p=0.0043$ ) and right hippocampus (4.3%,  $p=0.0001$ ), right amygdala (4.3%,  $p=0.0002$ ), and right thalamus (1.8%,  $p=0.0202$ ) for the ECT group. However, only the right hippocampus and right amygdala passed a Bonferroni correction ( $p<0.0026$ ). The TMS group showed a statistically significant volumetric increase in the right hippocampus (1.8%,  $p=0.0342$ ) and right thalamus (1.5%,  $p=0.0482$ ), but none of the areas passed the Bonferroni correction. The perfusion analy-

ses were combined for the Hippocampus, Amygdala, and Thalamus (HAT), because more gross changes were assumed compared to the volumetric changes. Still, the analyses were performed separately for the two hemispheres. There were no statistically significant changes between the groups at baseline perfusion, and none of the groups showed a statistically significant longitudinal increase or decrease. There were also no statistically significant differences across the hemispheres. Although not significant, there were trends showing a decrease in perfusion in the ECT group when investigating the rate of change in percent (%). Similarly, in the TMS group, trends showing a slight decrease followed by an increase were seen for the percent changes (%). There were also trends showing an increased baseline perfusion for the ECT group in both hemispheres. When more participants are included in the overall study, it can be verified whether these trends are true or random variations, as there were few participants at the time of the analysis and the perfusion data have larger variations than the volumetric data. The established pipeline can process image data from new participants as they join the study.

# Scientific environment

This study was conducted at the Department of Physics and Technology, University of Bergen. The work was done in collaboration with Mohn Medical Imaging and Visualization centre, Department of Radiology, Haukeland University Hospital, and The Neurostimulation and Brain Imaging Research Group (NBiG). Pipelines were developed at the Department of Physics and Technology, and computations were performed at clusters at the Department of Clinical Engineering, Haukeland University Hospital.



# Acknowledgements

I want to thank everyone who helped me with this project. I want to thank my main supervisor Renate Grüner for introducing me to the project, the interesting and helpful conversations with the analysis and writing, and for always motivating and reassuring me. I would also like to thank my co-supervisors, Frank Riemer and Leif Oltedal. Thank you, Frank, for helping me with practical problems and solutions, always providing humor, and making sure the project was manageable for a master thesis. Thank you, Leif, for your exciting conversations, for introducing me to the Neurostimulation and Brain Imaging Research Group (NBiG), for always providing good and constructive feedback, and all your help.

Thanks to the MMIV community, who have helped me through this project and for letting me present a poster (Appendix C) at the MMIV conference. Thank you to Erling Andersen for your invaluable help with the computations, Hauke Bartsch for all your technical help and discussions, Leila Marie Frid for your help with the dataset, and Njål Brekke for technical insights. I also want to thank the participants and the radiographers and radiologists at the Department of Radiology; this project could not have been done without you.

Thanks to the Neurostimulation and Brain Imaging Research Group (NBiG) for letting me present my project and for valuable tips and insight to neurostimulation, and to Ute Kessler for inviting me to the ECT Department. Visiting the department gave a greater understanding of the importance of my project.

I want to thank the students in room 534 for all your community and support. I would also like to thank my family, especially my mom Astrid Kleive and my dad Erling Andersen, for motivating me throughout this project, and to Henrik Steinli Træet for all the love and support.

Ingrid Kleive Andersen

Bergen, June 2024

# Contents

<b>Abstract</b>	<b>i</b>
<b>Scientific environment</b>	<b>iii</b>
<b>Acknowledgements</b>	<b>iv</b>
<b>Nomenclature</b>	<b>viii</b>
<b>List of Figures</b>	<b>x</b>
<b>List of Tables</b>	<b>x</b>
<b>1 Introduction</b>	<b>1</b>
<b>2 Theory</b>	<b>3</b>
2.1 Electromagnetism . . . . .	3
2.1.1 Electrical fields . . . . .	4
2.1.2 Magnetic fields . . . . .	6
2.1.3 Electrical conductivity of tissue . . . . .	6
2.2 Magnetic Resonance Imaging . . . . .	7
2.2.1 MRI Principles . . . . .	7
2.2.2 Perfusion through Arterial Spin Labeling . . . . .	22
2.2.3 Perfusion Physiology . . . . .	22
2.2.4 Perfusion Imaging . . . . .	22
2.3 Electromagnetic stimulation . . . . .	28
2.3.1 Electroconvulsive therapy . . . . .	28
2.3.2 Transcranial magnetic stimulation . . . . .	30

---

2.3.3	Application in mental disorders . . . . .	30
2.3.4	Biological effects and side effects . . . . .	32
2.4	Current knowledge . . . . .	32
2.5	Thesis motivation and aim . . . . .	34
<b>3</b>	<b>Methods</b>	<b>35</b>
3.1	Participants . . . . .	35
3.2	Treatment . . . . .	36
3.2.1	ECT . . . . .	36
3.2.2	TMS . . . . .	36
3.3	MRI acquisition . . . . .	36
3.4	MRI analysis . . . . .	37
3.4.1	FreeSurfer segmentation and longitudinal analysis . . . . .	38
3.4.2	Quantification of volumetric changes . . . . .	39
3.4.3	Quantification of perfusion changes . . . . .	40
3.5	Statistical analysis . . . . .	41
<b>4</b>	<b>Results</b>	<b>44</b>
4.1	Volume change . . . . .	45
4.1.1	Normal variation . . . . .	45
4.1.2	Variation across groups . . . . .	47
4.1.3	Effect of treatment . . . . .	47
4.2	Perfusion change . . . . .	53
4.2.1	Differences in baseline perfusion across groups . . . . .	53
4.2.2	Longitudinal perfusion change . . . . .	54
<b>5</b>	<b>Discussion and Conclusion</b>	<b>59</b>
5.1	Volume change . . . . .	59
5.1.1	Normal variation . . . . .	59
5.1.2	Variation across groups . . . . .	60
5.1.3	Effect of treatment . . . . .	60
5.2	Perfusion change . . . . .	62
5.2.1	Differences in baseline perfusion across groups . . . . .	62
5.2.2	Longitudinal perfusion change . . . . .	63



---

5.3	Potential confounders . . . . .	64
5.3.1	Dataset . . . . .	64
5.3.2	Treatment . . . . .	65
5.3.3	MRI Considerations . . . . .	65
5.3.4	Considerations of volume segmentation . . . . .	65
5.3.5	Considerations of perfusion estimation . . . . .	65
5.4	Conclusion and future work . . . . .	66
<b>Appendices</b>		<b>76</b>
<b>A Additonal tables</b>		<b>76</b>
A.1	Relative volumetric values for the control group . . . . .	76
A.2	Relative volumetric values for the ECT group . . . . .	77
A.3	Relative volumetric values for the TMS group . . . . .	78
<b>B Scripts</b>		<b>79</b>
<b>C Poster for the MMIV conference</b>		<b>80</b>

# Nomenclature

## Acronyms

**ASL** Arterial Spin Labeling

**BD** Bipolar Disorder

**BF** Bifrontal

**BT** Bitemporal

**cASL** Continous ASL

**CBF** Cerebral Blood Flow

**CSF** Cerebrospinal Fluid

**ECT** Electroconvulsive Therapy

**GEMRIC** Global ECT-MRI Research Collaboration

**GM** Grey Matter

**HAT** Hippocampus, Amygdala, and Thalamus

**LART** Left Anterior Right Temporal

**MADRS** Montgomery-Åsberg Depression Rating Scale

**MDD** Major Depressive Disorder

**MP-RAGE** Magnetization-Prepared Rapid Gradient Echo

**MRI** Magnetic Resonance Imaging

**pASL** Pulsed ASL

**pcASL** Pseudo-Continuous ASL

**PET** Positron Emission Tomography

**PLD** Post-Labeling Delay

**RF** Radio Frequency

**ROI** Region Of Interest

**RUL** Right Unilateral

**SNR** Signal-to-noise ratio

**SPECT** Single-Photon Emission Computed Tomography

**TE** Echo Time

**TES** Transcranial Electrical Stimulation

**TI** Inversion Time

**TMS** Transcranial Magnetic Stimulation

**TR** Repetition Time

**TRD** Treatment-Resistant Depression

**WM** White Matter

# List of Figures

2.1	Electric field lines for different charges . . . . .	5
2.2	The magnetic field lines of two magnetic dipoles . . . . .	6
2.3	The hydrogen atom with poles and magnetic field lines . . . . .	8
2.4	Excitating the proton in the fixed <b>(a)</b> and primed <b>(b)</b> frame. Modified figure from [21] . . . . .	10
2.5	The regrowth of the longitudinal magnetization. . . . .	13
2.6	The decay of the transverse magnetization. . . . .	14
2.7	The magnetization over time in all three directions. Modified figure from [21] .	15
2.8	Induction of current $\vec{I}$ in a coil by the magnetic moment $\vec{M}$ in a coil. Modified figure from [27]. . . . .	19
2.9	Sequence diagram for the MP RAGE sequence. Modified figure from [26] . . .	21
2.10	Simple illustration of the principles of ASL: labeling the water and subtracting the label from the control image. The labeled image <b>(b)</b> is subtracted from the control image <b>(a)</b> to create the perfusion map <b>(c)</b> . Modified figure from [28] . .	23
2.11	Simple illustration of a brief pulse stimulus. . . . .	29
2.12	The working mechanisms of TMS. The current in the TMS coil <b>(a)</b> induces a magnetic field <b>(b)</b> . The field has a rate of change <b>(c)</b> , which induces an electric field <b>(d)</b> and current <b>(e)</b> in the tissue. Modified figure from [14] . . . . .	30
3.1	A flowchart showing the MRI acquisitions for the different groups. The times-tamps are the time before or after the first treatment. All participants were scanned at 08:00, except at scan 2, performed at 12:00. . . . .	37

3.2	An illustration of the data processing. The T1 images were segmented using FreeSurfer, and the masks were used on the CBF maps to calculate the perfusion in the areas. <b>(a)</b> Sample images to show the analysis using FreeSurfer and FSL BASIL. The MRI machine calculates the CBF map based on label and control. The masks are of the left and right hippocampus. <b>(b)</b> The FreeSurfer and FSL BASIL commands used to analyze the images. The entries with borders are images and files, while the rest are commands. . . . .	37
4.1	Boxplot showing the variation of total intracranial volume between the groups .	47
4.2	The volumetric measurements for left hippocampus in the ECT group. . . . .	49
4.3	The volumetric measurements for right hippocampus in the ECT group. . . . .	49
4.4	The volumetric measurements for right amygdala in the ECT group. . . . .	50
4.5	The volumetric measurements for right thalamus in the ECT group. . . . .	50
4.6	The volumetric measurements for Right Hippocampus in the TMS group. . . . .	52
4.7	The volumetric measurements for Right Thalamus in the TMS group. . . . .	52
4.8	Perfusion in left <b>(a)</b> and right <b>(b)</b> Hippocampus, Amygdala, and Thalamus (HAT) at Scan 1. . . . .	53
4.9	Plot of the perfusion in left and right Hippocampus, Amygdala and Thalamus (HAT) over time for the control group . . . . .	55
4.10	Plot of the perfusion in left and right Hippocampus, Amygdala and Thalamus (HAT) over time for the ECT group . . . . .	56
4.11	Plot of the perfusion in left and right Hippocampus, Amygdala and Thalamus (HAT) over time for the TMS group . . . . .	57
C.1	The poster presented at the MMIV conference for the project in December 2023	81

# List of Tables

2.1	Conductivity of different tissues and materials. The numbers are found in articles by Wagner [24] and Datta [25]. . . . .	7
3.1	Information about the study participants across the three groups. std = standard deviation, N = number of participants. . . . .	36
4.1	Mean value, standard deviation, percent change from scan 1 to scan 4 and p-value for the volumes in the ROIs for the control group. WM=White Matter, std=Standard Deviation . . . . .	46
4.2	Mean value ( $mm^3$ ) and standard deviation ( $mm^3$ ) of the total intracranial volume across the three groups. . . . .	47
4.3	Mean value, standard deviation, percent change from scan 1 to scan 4 and p-value for the volumes in the ROIs for the ECT group. . . . .	48
4.4	Mean value, standard deviation, percent change from scan 1 to scan 4 and p-value for the volumes in the ROIs for the TMS group. WM=White Mater, std=Standard Deviation . . . . .	51
4.5	t-value and p-value for the difference in perfusion between the control group and the ECT group or the TMS group, respectively, for the left (a) and right (a) hippocampus, amygdala and thalamus. . . . .	54
4.6	Mean value of CBF in hippocampus, amygdala, and thalamus (HAT) and the laterality index in percent for the control group . . . . .	54
4.7	Mean value of CBF in HAT and the laterality index in percent for the ECT group	55
4.8	Mean value of CBF in HAT and the laterality index in percent for the TMS group	57
4.9	t-value and p-value for the change between scan 1 and scan 4 in the control, ECT, and TMS group, respectively. . . . .	58

---

A.1	Relative mean value, standard deviation and p-value for the volumes in the ROIs for the control group. WM = White Matter, std = Standard Deviation . . . . .	76
A.2	Relative mean value, standard deviation and p-value for the volumes in the ROIs for the ECT group. WM = White Matter, std = Standard Deviation . . . . .	77
A.3	Relative mean value, standard deviation and p-value for the volumes in the ROIs for the TMS group. WM = White Matter, std = Standard Deviation . . . . .	78





# Chapter 1

## Introduction

### **Major Depressive Disorder and Bipolar Disorder**

Major Depressive Disorder (MDD) is a common mental disorder, affecting approximately 280 million people worldwide. MDD is characterized by experiencing a depressed mood and thoughts of hopelessness or suicide, that last most of the day, nearly every day for more than two weeks. [1]. In 2019 MDD was ranked by The Lancet as the 4th largest contributor in the world in the number of healthy years lost due to disability (YLDs) [10]. Bipolar Disorder (BD) is a mental illness that causes changes in a person's mood, energy and activity levels. The mood ranges from manic, which is characterized by energized, irritable or happy moods, to depressed, which is characterized by hopelessness, indifference or sad moods. People with BD might also experience mixed episodes with both manic and depressive symptoms, as well as catatonia, which is characterized by immobility, stupor and rigidity [2].

### **Electroconvulsive Therapy and Transcranial Magnetic Stimulation**

Electroconvulsive Therapy (ECT) is a treatment option for Treatment-Resistant Depression (TRD), which is experienced by approximately 30% of patients with MDD [3], as well as BD [11]. ECT is very effective for treating a depressive episode, with over 50% of patients with TRD responding to the treatment [3]. ECT is performed by applying a series of brief electrical pulses via electrodes attached to the scalp, inducing a seizure. Side effects include temporary memory loss and difficulty with learning [12]. Transcranial Magnetic Stimulation (TMS) is another treatment option for TRD [4] and BD [2]. TMS uses a coil to induce a magnetic field that passes through the scalp [13], leading to the stimulation of neurons in the brain[14].

**Volume change**

A typical biological effect after ECT treatment is volume change in selected brain areas like the hippocampus [15]. The underlying mechanisms of ECT are not entirely understood [16]. Some models suggest that a decrease in neurogenesis in the Hippocampus is associated with depression and can potentially be reversed by ECT [15]. Volume changes are not restricted to the hippocampus and can be found in most Grey Matter (GM) areas following ECT [17] [18].

**Perfusion may explain volumetric changes**

Investigating the intensity of the brain microvasculature through brain perfusion imaging is sparse in ECT research. A study from 2019 assessed the correlation between cerebral perfusion and clinical outcome and found that patients with a lower baseline global perfusion were more likely to respond to ECT [19]. Another study from 2023 found a correlation between seizure duration and regional perfusion after the treatment [20]. A third study from 2021 studied the role of hippocampal plasticity in antidepressant response to ECT and found that non-responders had increased CBF in the bilateral anterior hippocampus, while responders had increased CBF in the right middle and left posterior hippocampus [7].

**Aim of this study**

This project aims to investigate if there is a connection between changes in brain perfusion and volume changes in areas in the brain. The hypothesis is that the ECT treatment will increase volume in specific brain areas and that these areas will have an altered perfusion.

**Contributions**

Finding a connection between brain perfusion and volume change can improve understanding of the ECT working mechanisms. It can contribute to our understanding of how the volume increases happen and why.

# Chapter 2

## Theory

In this chapter, concepts of electromagnetism, Magnetic Resonance Imaging (MRI), ECT, and TMS are explained. Understanding the theory and physical principles behind the treatment and imaging methods is essential to understanding the applied methods and the results.

### 2.1 Electromagnetism

All electromagnetic fields follow Maxwell's equations. Equation (2.2) is called Gauss's law, equation (2.3) is called Faraday's law, and equation (2.4) is called Ampere's law. [21]

$$\vec{\nabla} \cdot \vec{B} = 0 \quad (2.1)$$

$$\vec{\nabla} \cdot \vec{D} = \rho_q \quad (2.2)$$

$$\vec{\nabla} \times \vec{E} + \frac{\partial \vec{B}}{\partial t} = 0 \quad (2.3)$$

$$\vec{\nabla} \times \vec{H} = \vec{J} + \frac{\partial \vec{D}}{\partial t} \quad (2.4)$$

Here,  $\vec{D} = \epsilon \vec{E}$ ,  $\vec{B} = \mu \vec{H}$ .  $\epsilon$  is the dielectric constant and  $\vec{E}$  is the electric field strength.  $\vec{B}$

is the magnetic flux density,  $\mu$  is the permeability and  $\vec{H}$  is the magnetic field strength.  $\rho_q$  is the electric charge density, and  $\vec{J}$  is the electric current density as current per unit area. [21].

The integral form of Faraday's law (2.5) is called Faraday's law of induction. Equation 2.6 describes the magnetic flux through a surface  $S$ . Equation 2.7 describes the electromotive force  $\varepsilon$  induced in the case where the surface is bounded by a wire loop. If 2.6 and 2.7 are substituted into 2.5, the result is the more familiar version of Faraday's law (2.8). [21]

$$\oint \vec{E} \cdot d\vec{l} = -\frac{d}{dt} \left( \int \vec{B} \cdot d\vec{S} \right) \quad (2.5)$$

$$\Phi_B = \int \vec{B} \cdot d\vec{S} \quad (2.6)$$

$$emf = \oint \vec{E} \cdot \vec{l} \quad (2.7)$$

$$emf = -\frac{d\Phi_B}{dt} \quad (2.8)$$

Equation 2.8 states that a time-varying magnetic flux through a circuit generates a voltage with amplitude proportional to the negative rate of change of the flux. Or, a voltage is induced if the flux of the magnetic field varies. Such time-varying magnetic fields are what is recorded in MRI, which will be further explained in section 2.2. [21]

### 2.1.1 Electrical fields

Coulomb's law 2.9 describes the force on a test charge  $Q$  to a single point charge  $q$  at rest at distance  $r$  away. [22]

$$\vec{F} = \frac{1}{4\pi\epsilon_0} \frac{qQ}{r^2} (\vec{\hat{r}}) \quad (2.9)$$

In equation 2.9 the constant  $\epsilon_0$  is the permittivity of free space, and has the value  $\epsilon_0 = 8.85 \cdot 10^{-12} C^2/N \cdot m^2$ . The vector  $\vec{\hat{r}}$  is direction from  $q$  to  $Q$ . [22]

If there are several point charges  $q_1, q_2, \dots, q_n$  at distances  $r_1, r_2, \dots, r_n$  from  $Q$ , then the total force on  $Q$  is described in equation 2.10, and can be summed up in equation 2.11. Equation 2.12 describes the variable  $\vec{E}(\vec{r})$ , which is the electrical field of the source charges.  $\vec{E}$  is a function of position  $\vec{r}$  which is the location of the test charge  $Q$ . [22]

$$\begin{aligned}\vec{F} &= \vec{F}_1 + \vec{F}_2 + \dots + \vec{F}_n \\ &= \frac{1}{4\pi\epsilon_0} \left( \frac{q_1 Q}{r_1^2} \vec{r}_1 + \frac{q_2 Q}{r_2^2} \vec{r}_2 + \dots + \frac{q_n Q}{r_n^2} \vec{r}_n \right) \\ &= \frac{Q}{4\pi\epsilon_0} \left( \frac{q_1}{r_1^2} \vec{r}_1 + \frac{q_2}{r_2^2} \vec{r}_2 + \dots + \frac{q_n}{r_n^2} \vec{r}_n \right)\end{aligned}\quad (2.10)$$

$$\vec{F} = Q\vec{E} \quad (2.11)$$

$$\vec{E}(\vec{r}) := \frac{1}{4\pi\epsilon_0} \sum_{i=1}^n \frac{q_i}{r_i^2} \vec{r}_i \quad (2.12)$$

Electric field lines are used to visually describe the electric field  $\vec{E}$ . They are drawn as curves or lines, in such a way that the tangent at any point is the direction of  $\vec{E}$ . The field lines also give an indicator of the strength of the field. If  $\vec{E}$  is strong the lines are drawn closer together, and if  $\vec{E}$  is weak they are drawn far apart. [23] This is shown in figure 2.1. The closer you are to the source of the charge  $Q$ , the closer the field lines, and the larger  $\vec{E}$ . This corresponds well with equation 2.12, which describes  $\vec{E}$  as a function of position  $\vec{r}$

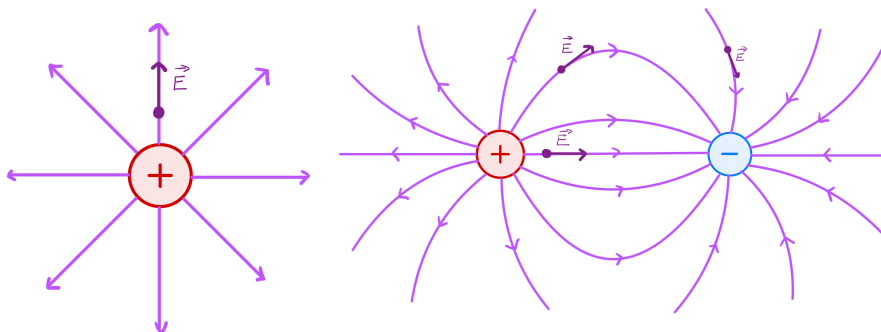


**Figure 2.1:** Electric field lines for different charges

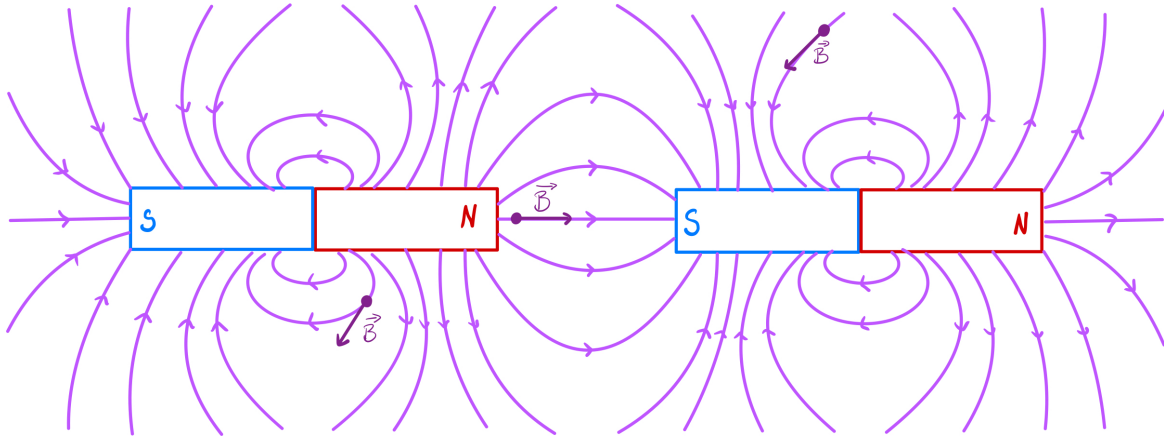


*Figure 2.2: The magnetic field lines of two magnetic dipoles*

### 2.1.2 Magnetic fields

An electric charge immersed in an electric field  $\vec{E}$  or moving through a magnetic field  $\vec{B}$  will experience electromagnetic forces. This force from  $\vec{E}$  is proportional and parallel to  $\vec{E}$ . The force from  $\vec{B}$  on the other hand, is perpendicular to the particle's velocity and the direction of  $\vec{B}$ . It is determined by the right hand as described by equation 2.13. [21]

$$\vec{F} = q\vec{E} + q\vec{v} \times \vec{B} \quad (2.13)$$

The magnetic field can, like the electric field, be visualized using field lines. They are drawn as curves or lines in such a way that the tangent at any point is the direction of  $\vec{B}$ . [23]. Figure 2.2 show the field lines of two magnetic dipoles, and the direction of  $\vec{B}$  at a few selected points.

### 2.1.3 Electrical conductivity of tissue

An important property of a material is conductivity. It is an empirical constant that gives information about how easily a current can move through a material. Equation 2.14 shows how the current density  $\vec{J}$  depends on the conductivity and force per unit charge  $\vec{f}$ . A good conductor like metal will have a high conductivity, and a bad conductor like an insulator will have low conductivity. [22]

$$\vec{J} = \sigma \vec{f} \quad (2.14)$$

The data in table 2.1 are collected from the articles by Wagner [24] and Datta, and show the conductivities for different tissues and materials relevant for ECT and TMS [25].

**Table 2.1:** Conductivity of different tissues and materials. The numbers are found in articles by Wagner [24] and Datta [25].

Material	Conductivity (S/m)
Skin	0.465
Bone	0.01
CSF	1.654
GM	0.276
WM	0.126
Brain	0.2
Gel	0.3
Electrodes	$5.8 \times 10^7$

## 2.2 Magnetic Resonance Imaging

In order to understand the effects of treatment using TMS and ECT, neuroimaging using MRI is applied. The basic principles of MRI are described next. Both classical and quantum mechanical descriptions are used to explain the principles of MRI.

### 2.2.1 MRI Principles

#### The nucleus and the magnetic field

The hydrogen nucleus is the most commonly used in MRI. The interaction of the hydrogen nucleus with external magnetic fields gives rise to the MRI signal. The interaction between the hydrogen nucleus and the magnetic fields causes a clockwise precession of the proton around the direction of the magnetic field lines, see figure 2.3. The precession causes an electric current around its axis, which can interact with, and create its own magnetic field. The strength of the interaction and the new field is called magnetic dipole moment ( $\mu$ ), and will align itself along the external magnetic field. [21]

#### Magnetic moment

To understand how the magnetic moment acts in the presence of a magnetic field, we imagine a circular loop with current  $I$  and area  $A$ . If an external magnetic field  $\vec{B}_0$  is turned on, each length segment  $d\vec{l}$  will feel a force given by the Lorentz force law (2.13). Equation 2.15 shows how the force in the segment  $d\vec{l}$  is perpendicular to the segment and the magnetic field at the

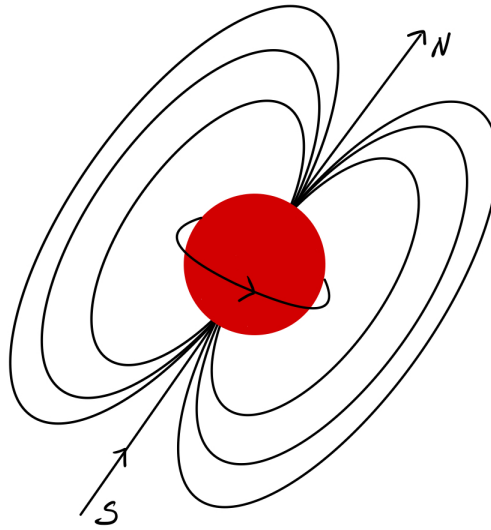


**Figure 2.3:** The hydrogen atom with poles and magnetic field lines

segment. With a uniform magnetic field, the total force on the loop is zero. [21]

$$d\vec{F} = I d\vec{l} \times \vec{B} \quad (2.15)$$

The loop can be rotated by  $\vec{B}_0$  depending on the loops' orientation even if the vector sum of the forces cancel each other out, as long as the force is applied off-center. The net torque  $\vec{N}$  is the sum of the torque contributions, as described in equation 2.16. If there is a non-zero total torque  $\vec{N}$ , the angular momentum of the system must change as described in equation 2.17. The relationship between the magnetic moment and angular momentum is described in equation 2.18. [21]

$$\vec{N} = \vec{\mu} \times \vec{B} \quad (2.16)$$

$$\frac{d\vec{J}}{dt} = \vec{N} \quad (2.17)$$

$$\vec{\mu} = \gamma \vec{J} \quad (2.18)$$

If equation 2.16 and 2.17 is substituted into 2.18, the resulting equation (2.19) describes the



motion of the spin. [21]

$$\frac{d\vec{\mu}}{dt} = \gamma\vec{\mu} \times \vec{B} \quad (2.19)$$

### The principles of resonance

The principles of resonance can be described using rotating reference frames. The fixed reference frame is denoted by cartesian coordinates  $x$ ,  $y$  and  $z$ , and the rotating reference frame is denoted by the primed cartesian coordinates  $x'$ ,  $y'$  and  $z'$ . Consider a vector  $\vec{V}$  not at rest and time-dependent in both the fixed and primed reference frame. It has an angular velocity  $\vec{\Omega}$ . Equation 2.20 and 2.21 shows  $\vec{V}$  as a combination of its unit vectors, in the fixed and primed reference frame, respectively. Solving equation 2.20 and 2.21 gives the time derivative for the fixed and primed reference frame. Equation 2.22 and 2.23 shows the solutions, respectively. [21]

$$\vec{V}(t) = V_x(t)\hat{x} + V_y(t)\hat{y} + V_z(t)\hat{z} \quad (2.20)$$

$$\vec{V}'(t) = \vec{V}(t) = V_{x'}(t)\hat{x}' + V_{y'}(t)\hat{y}' + V_{z'}(t)\hat{z}' \quad (2.21)$$

$$\frac{d\vec{V}}{dt} = \left(\frac{d\vec{V}}{dt}\right)' + \vec{\Omega} \times \vec{V} \quad (2.22)$$

$$\left(\frac{d\vec{V}}{dt}\right)' = \frac{dV_{x'}(t)}{dt}\hat{x}'(t) + \frac{dV_{y'}(t)}{dt}\hat{y}'(t) + \frac{dV_{z'}(t)}{dt}\hat{z}'(t) \quad (2.23)$$

Consider the magnetization vector  $\vec{\mu}$  as the vector  $\vec{V}$ . Equation 2.24 describes the rate in the fixed frame. If equation 2.19 is used to substitute the rate in the fixed frame, the rate in the primed frame is described by equation 2.25. The effective magnetic field ( $B_{eff}$ ) in the rotating field is described in equation 2.26. By choosing the rate of the primed frame  $\vec{\Omega}$ , one can express the motion of the magnetic moment favorably. [21]

$$\frac{d\vec{\mu}}{dt} = \left( \frac{d\vec{\mu}}{dt} \right) + \vec{\Omega} \times \vec{\mu} \quad (2.24)$$

$$\left( \frac{d\vec{\mu}}{dt} \right)' = \gamma\mu \times \vec{B}_{eff} \quad (2.25)$$

$$\vec{B}_{eff} = \vec{B} + \frac{\vec{\Omega}}{\gamma} \quad (2.26)$$

### Excitation with the RF pulse

To excite the nucleus, Radio Frequency (RF) pulses are applied. The RF pulse needs components in the x and y-direction to tip the nucleus away from the z-direction. To knock the spin out of place, one must apply a force at the same place in the precessional path. As a wave-form pulse is applied, the frequency of the pulse needs to have the same frequency as the precessional path. This gives a new equation of motion in the primed reference frame for the nucleus, described in equation 2.27, where  $\omega_0$  is the Larmor frequency for the  $\vec{B}_0$ ,  $\omega$  is the frequency of the RF pulse, and  $\omega_1$  is the precession frequency generated by the RF pulse. In the special case where the frequency of the RF pulse is equal to the Larmor frequency,  $\omega = \omega_0$ , equation 2.27 gives equation 2.28. The nucleus will then have a precession around the  $\hat{x}'$ -axis with a frequency of  $\omega_1$ . This then shows how the resonance occurs if the frequency of the applied RF pulse is the same as the Larmor frequency. [21] Figure 2.4 shows how the precessional path looks for both the fixed and the primed reference frame.

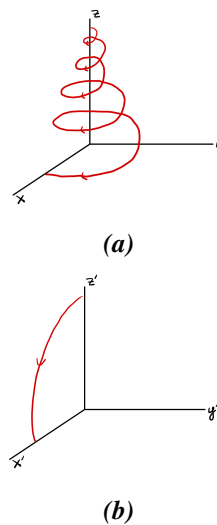


**Figure 2.4:** Excitating the proton in the fixed (a) and primed (b) frame. Modified figure from [21]

$$\left(\frac{d\vec{\mu}}{dt}\right)' = \vec{\mu} \times [\hat{z}'(\omega_0 - \omega) + \hat{x}'\omega_1] \quad (2.27)$$

$$\left(\frac{d\vec{\mu}}{dt}\right)' = \omega_1 \vec{\mu} \times \hat{x}' \quad (2.28)$$

If the pulse is only on for a short time interval  $\tau$ , the nucleus will not tip over to the  $\hat{x}'$ -axis, but only get an angle from the  $\hat{z}'$ -axis, the so-called flip angle ( $\alpha$ ). The angle is described by equation 2.29. [21]

$$\Delta\alpha = \gamma B_1 \tau \quad (2.29)$$

### Magnetization, relaxation and the Bloch equation

The spin of a single proton is too small to be measured, so instead the net magnetization of a voxel is measured. The net magnetization vector ( $\vec{M}$ ) is the sum of the magnetic moment from each nucleus in the voxel, as described by equation 2.30. For non-interactive protons, the motion of the collection of spins is described by equation 2.31, where  $\vec{B}_e$  is the external magnetic field. If the direction of the  $\vec{B}_e$  is along the  $\hat{z}$ -direction, the motion can be divided into parallel (2.32) and orthogonal (2.33) components for non-interacting protons. [21]

$$\vec{M} = \frac{1}{V} \sum_i^N \vec{\mu}_i \quad (2.30)$$

$$\frac{d\vec{M}}{dt} = \gamma \vec{M} \times \vec{B}_e \quad (2.31)$$

$$\frac{dM_{||}}{dt} = 0 \quad (2.32)$$

$$\frac{d\vec{M}_{\perp}}{dt} = \gamma \vec{M}_{\perp} \times \vec{B}_e \quad (2.33)$$

### Thermal equilibrium and longitudinal relaxation

Only a small fraction of the protons align with the magnetic field. To explain this, the energy

aspect of interacting protons is studied. The potential energy for the  $\vec{M}$  (2.34) shows how the lowest energy state for the protons is parallel to the external magnetic field. To line up with the field, the nuclei give away thermal energy to the nearby atoms. The longitudinal magnetization reaches an equilibrium, called initial magnetization  $M_0$ , described by Curie's law (2.35), where  $T$  is the absolute temperature. This magnetization is very small compared to the largest possible magnetization, and the energy associated with this state is relatively small compared to, say, the thermal energy at room temperature. It is therefore only a small advantage to align with the field, and there will only be an excess of around 5 in a million of a 1.5T field. However, in a voxel, there are a lot of protons ( $\approx 10^8$ ), so the  $M_0$  signal becomes detectable. [21]

$$U_M = -\vec{M} \cdot \vec{B} = -M_{||}B_0 \quad (2.34)$$

$$M_0 = C \frac{B_0}{T} \quad (2.35)$$

### T1 relaxation

When the magnetic moment of the proton is pushed away from the  $\vec{B}_0$  by the RF pulse, it will return to the equilibrium  $M_0\hat{z}$ . This, however, does not happen instantaneously. Equation 2.36 shows how the rate of change of longitudinal magnetization is proportional to the difference  $M_0 - M_z$ . The constant  $T_1$  is empirically determined and is called the spin-lattice relaxation time. It has different values depending on what type of tissue is affected by the  $\vec{B}_0$ -field, ranging from 250ms for fat to 4500 for Cerebrospinal Fluid (CSF) at a  $\vec{B}_0=1.5\text{T}$  at body temperature. By solving equation 2.36, the result is equation 2.37. In the special case where  $M_z(0) = 0$ , the magnetization can be rewritten into equation 2.38. [21]. Figure 2.5 shows how the longitudinal magnetizations regrow over time.

$$\frac{dM_z}{dt} = \frac{1}{T_1}(M_0 - M_z) \quad (2.36)$$

$$M_z(t) = M_z(0)e^{-t/T_1} + M_0(1 - e^{-t/T_1}) \quad (2.37)$$

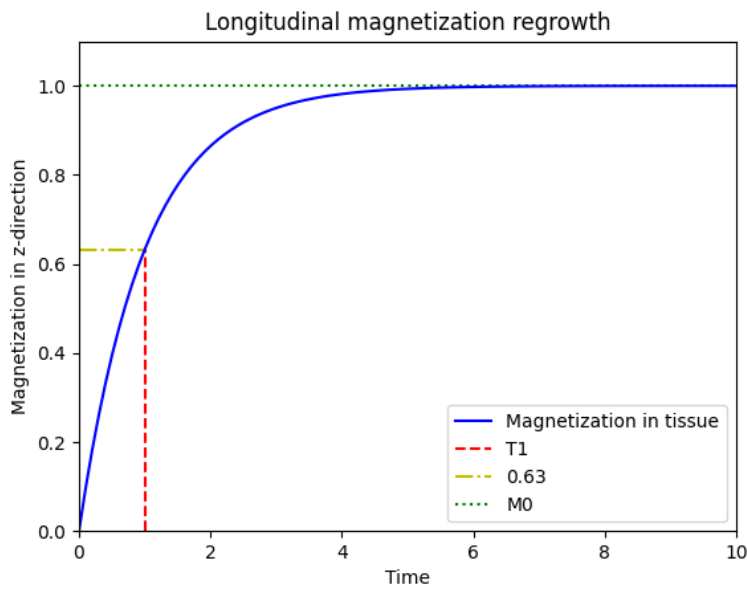


*Figure 2.5: The regrowth of the longitudinal magnetization.*

$$M_z(t) = M_0(1 - e^{-t/T_1}) \quad (2.38)$$

The longitudinal relaxation is the foundation of T1-weighted images. In these images, tissue with short T1 times gives the strongest signal. The images have good contrast between different tissues, making them excellent anatomical images. [26]

### T2 relaxation

As the magnetization regains strength in the z-direction, the magnetization in the x-y plane decreases. The spin of the nucleus is affected by the spins of the surrounding nuclei, and the individual precessional frequencies fall out of sync. The net magnetization becomes smaller as the total signal becomes more dispersed. Equation 2.39 shows the rate of change of transverse magnetization, and equation 2.40 shows equation 2.39 for a rotating reference frame. The parameter  $T_2$  is called the spin-spin relaxation time. The solution to equation 2.40 is shown in equation 2.41. [21]. Figure 2.6 shows the decay of the transverse magnetization over time.

$$\frac{d\vec{M}_\perp}{dt} = \gamma\vec{M}_\perp \times \vec{B}_e - \frac{1}{T_2}\vec{M}_\perp \quad (2.39)$$

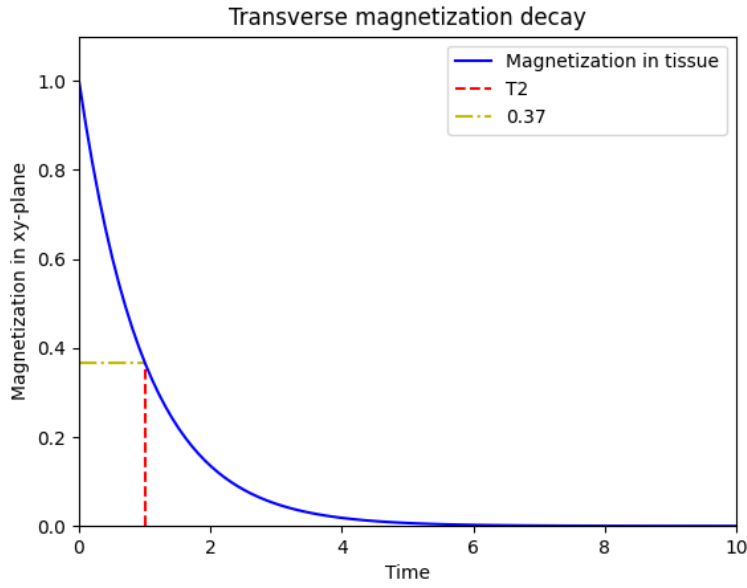


**Figure 2.6:** The decay of the transverse magnetization.

$$\left( \frac{d\vec{M}_{\perp}}{dt} \right)' = -\frac{1}{T_2} \vec{M}_{\perp} \quad (2.40)$$

$$\vec{M}_{\perp}(t) = \vec{M}_{\perp}(0) e^{-t/T_2} \quad (2.41)$$

The transverse magnetization is the foundation for T2-weighted images. Tissues with longer T2 relaxation times give stronger signals, and the images take longer to acquire. The images easily pick up on fluid collections, making them great as diagnostic tools. [26]

To describe more in details what happens to the net magnetization vector, equation 2.36 and 2.39 are combined into equation 2.42. If the magnetic field  $\vec{B}_0$  goes along the z-direction, equation 2.42 can be split up into its three components. When solving for  $M$  and calculating what happens to the magnetization over time, one finds that  $M_x(\infty) = M_y(\infty) = 0$  and  $M_z(\infty) = M_0$  or the magnetization in the x-y plane goes to 0 and the magnetization in the z-direction goes to  $M_0$ . [21] This movement is shown in figure 2.7.

$$\frac{d\vec{M}}{dt} = \gamma \vec{M} \times \vec{B}_e + \frac{1}{T_1} (M_0 - M_z) \hat{z} - \frac{1}{T_2} \vec{M}_{\perp} \quad (2.42)$$

## Energy states

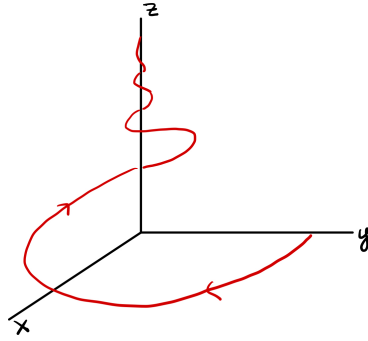


**Figure 2.7:** The magnetization over time in all three directions. Modified figure from [21]

The nuclei have different energy states depending on their spin. This principle was described through an experiment by Stern and Gerlach in the 1920's. Consider a beam of non-charged silver nuclei traveling along the x-axis through a non-homogenous magnetic field along the z-axis. Because of the magnetic moment, they are affected by the magnetic field by a force described in equation 2.43. The y-component of the force will cancel out over time, and the force can be rewritten as equation 2.44. This equation describes a gradient, which will be discussed later. In the silver atom, there is an unpaired electron with an angular momentum which gives rise to an atomic magnetic moment 2.45. The component of this moment that is parallel to the field will deflect. [21]

$$\vec{F} = -\vec{\nabla}U = \vec{\nabla}(\vec{\mu} \cdot \vec{B}) \quad (2.43)$$

$$F_z = \mu_z \frac{\partial B}{\partial z} = \mu_z G_z \quad (2.44)$$

$$\vec{\mu}_e = \gamma_e \vec{J}_e \quad (2.45)$$

Classically, the beam should be deflected continuously. However during this experiment, one finds that the beam is split into two beams. These beams correspond to the two discrete values the angular momentum has in the z-direction. The values for angular momentum are described in equation 2.46, [21]

$$J_z = m_j \hbar = m_j \frac{h}{2\pi} \quad (2.46)$$

where  $j$  is the quantum number and is either integer or half-integer,  $m_j = -j, -j+1, \dots, j-1, j$  is the magnetic quantum number, and  $h$  is Planck's constant. The magnetic moment has two contributors: the orbital spin and the intrinsic spin. The orbital spin can be compared with how the Earth goes around the sun, and intrinsic spin is how the Earth spins around itself. Orbital spin has integer quantum numbers and intrinsic spin has integer and half-integer quantum numbers. If there is no orbital spin, as for protons in matter, the quantum number is  $s = \frac{1}{2}$  and the magnetic quantum number is  $m_s = \pm \frac{1}{2}$ . Because of this, the protons have discrete magnetic moment values and discrete energy values, as described in equation 2.47. [21]

$$E = -\vec{\mu} \cdot \vec{B} = -\gamma m_s \hbar B_z \quad (2.47)$$

If we now look at the required energy to transition from a lower energy state to a higher energy state, it connects well with the classical interpretation. Equation 2.48 shows how the required energy corresponds to a wave with the Larmor frequency. [21]

$$\Delta E = E\left(m_s = -\frac{1}{2}\right) - E\left(m_s = \frac{1}{2}\right) = \frac{1}{2}\gamma\hbar B_0 - \left(\frac{1}{2}\gamma\hbar B_0\right) = \gamma\hbar B_0 = \hbar\omega_0 \quad (2.48)$$

### Thermal equilibrium

To find the constant  $C$  from Curie's law (2.35), consider a proton in a magnetic field. The force on the proton is described in equation 2.13. As the force is perpendicular to the velocity the force will not affect it, but other surrounding effects like radiation will eventually stop the particle as it gives off its energy to the surroundings. If, however, the particle is in thermal contact with another material, some kinetic energy will be retained in the order of  $kT$ , where  $k$  is Boltzmann's constant and  $T$  is the absolute temperature. The equilibrium will be a little above the lowest energy state, depending on  $kT$ . The normalized Boltzmann factor describes the probability of finding a system with energy  $\varepsilon$  that is in contact with a larger system at temperature  $T$  (2.49). [21]

$$P(\varepsilon) = \frac{e^{-\varepsilon/kT}}{\sum_{\varepsilon} e^{-\varepsilon/kT}} \quad (2.49)$$

The system in this case is a spin that is in thermal contact with other  $N-1$  spins and the background lattice at temperature  $T$ . To find  $M_0$ , the z-component of the average total magnetic



moment for all  $N$  spins for all possible spin states is calculated. If choosing the axis along  $\vec{B}_0$  and a spin  $s$  with a magnetic number  $m_s$ , the thermal average is described by equation 2.50. [21]

$$M_0 = \rho_0 \sum_{m=-s}^s P(\varepsilon(m_s)) \mu_z(m_s) \quad (2.50)$$

By substituting  $\varepsilon = -m\hbar\omega_0$ ,  $\mu_z = m\gamma\hbar$ ,  $\rho_0 = N/V$  (density of spin), and considering the finite  $m$ -values of interest, an expression for  $M_0$  can be presented in equation 2.51. For a proton with spin  $s = 1/2$ , the equation for  $M_0$  is described in equation 2.52, with the constant  $C$  from Curie's law described in equation 2.53. All equations require  $\hbar\omega_0 \ll kT$ . [21]

$$M_0 \simeq \rho_0 \frac{s(s+1)\gamma^2\hbar^2}{3kT} B_0 \quad (2.51)$$

$$M_0 \simeq \frac{1}{4}\rho_0 \frac{\gamma^2\hbar^2}{kT} B_0 \quad (2.52)$$

$$C \simeq \frac{1}{4}\rho_0 \frac{\gamma^2\hbar^2}{k} \quad (2.53)$$

### Longitudinal relaxation

Consider  $N$  protons at rest in a constant magnetic field  $B_0\hat{z}$ . The protons can be in one of two spin states,  $m_s = 1/2$  and  $m_s = -1/2$ , with  $m_s$  corresponding to the lowest energy state parallel to the field. If a proton goes to a lower energy state, from  $m_s = -1/2$  to  $m_s = 1/2$ , it must also go from a lower lattice state to a higher lattice state to compensate for the energy loss. It goes from low state  $l-$  to high state  $h+$ . The process can also be reversed. The probability for a proton to switch lattice state is denoted  $W_{h+l-}$  for going to a higher lattice state, and  $W_{-lh+}$  for switching to a lower lattice state. The rate of change of protons switching from one state to the other is described in equation 2.54, where  $N_+$  is the initial number of spins in state  $m = 1/2$ ,  $n_h$  is the number of initial lattice states with higher energy and  $n_l$  is the number of initial lattice states with lower energy.  $n_h$  and  $n_l$  are related through the Boltzmann factor ratio, as described in equation 2.55. [21]

$$\frac{dN_+}{dt} = W_{h+l-}N_-n_l - W_{-lh+}N_+n_h \quad (2.54)$$

$$\frac{n_h}{n_l} = e^{-\gamma\hbar B_0/kT} \quad (2.55)$$

The probability for a proton to switch state is the same regardless of direction, and so  $W_{h+l-}$  and  $W_{l-h+}$  are the same and will be denoted  $W$ . If  $\Delta N$  is the spin excess in the  $B_0\hat{z}$  direction, equation 2.54 can be rewritten into equation 2.56. Solving for  $d\Delta N/dt = 0$  gives the equation for equilibrium. [21]

$$\frac{d\Delta N}{dt} = WN(n_l - n_h) - W\Delta N(n_l + n_h) \quad (2.56)$$

$$\Delta N_0 = \frac{n_l - n_h}{n_l + n_h} N \quad (2.57)$$

The value  $\Delta N$  is the spin-relaxation decay rate, which we already know as the T1 relaxation time. Equation 2.58 shows this relationship. The rate of change can be rewritten to equation 2.59, and by multiplying by the  $z$ -component,  $1/2\gamma\hbar$ , and averaging over volume, we get the rate of change for a proton along the  $z$ -axis and is the same as equation 2.36. [21]

$$\frac{1}{T_1} := W(n_l + n_h) \quad (2.58)$$

$$\frac{d\Delta N}{dt} = \frac{\Delta N_0 - \Delta N}{T_1} \quad (2.59)$$

$$\frac{dM_z}{dt} = \frac{M_0 - M_z}{T_1}$$

### The introduction of the RF field

When a RF field is turned on, it causes transitions between the two spin states. The probability for a proton to switch states is here denoted  $w$ , and is the same for switching from  $m_s = 1/2$  to  $m_s = -1/2$  and the opposite. The rate of change is described in equation 2.60 and equation 2.61. [21]

$$\frac{dN_+}{dt} = N_-w - N_+w \quad (2.60)$$

$$\frac{d\Delta N}{dt} = -2w\Delta N = \frac{\Delta N_0 - \Delta N}{T_1} - 2w\Delta N \quad (2.61)$$

### Signal detection

In Section 2.1 Electromagnetism, Faraday's law of induction was studied (2.8) along with the equation for flux through a coil (2.6). This law states that a flux *emf* can be induced in a coil by changing the magnetic flux through the coil. Consider a square coil in a time-dependent sinusoidal magnetic field. The field has angular frequency  $\omega$  at an angle  $\theta$  to the normal of the plane of the coil and is constant at a fixed time  $t$ . The magnetic field is given by equation 2.62. If the coil is located in the  $x$ - $y$  plane, the induced *emf* is described in equation 2.63. Figure 2.8 shows how the magnetic moment induces a current  $\vec{I}$  in a circular coil. [21]

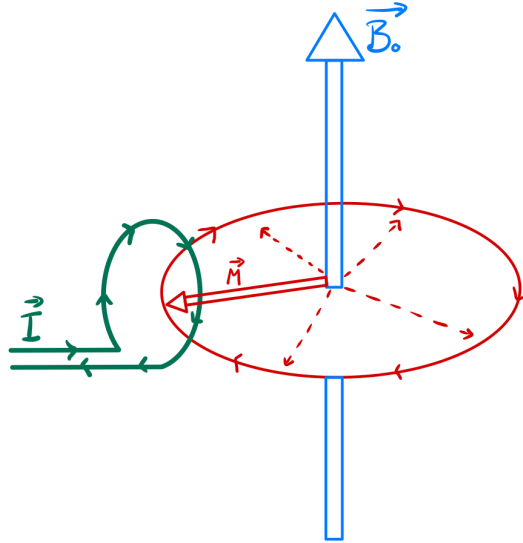


**Figure 2.8:** Induction of current  $\vec{I}$  in a coil by the magnetic moment  $\vec{M}$  in a coil. Modified figure from [27].

$$\vec{B}(t) = B(\sin(\theta)\hat{y} + \cos(\theta)\hat{z})\sin(\omega t) \quad (2.62)$$

$$emf = -\frac{d}{dt} \int_{-L/2}^{L/2} dx \int_{-L/2}^{L/2} dy \hat{z} \cdot \vec{B}(t) = -L^2 b \omega \cos(\theta) \cos(\omega t) \quad (2.63)$$

The field we want to measure in MRI is the magnetization  $M$ . This magnetization has a current density  $\vec{J}$  associated with it, as described in equation 2.64. The current density implies  $|\vec{J}|$  charge per unit time per unit area in the  $\vec{J}$  direction. The vector potential  $\vec{A}$  at position  $\vec{r}$  from a source current is described in equation 2.65. Using  $\vec{B} = \vec{\nabla} \times \vec{A}$  as the magnetic field, one can calculate the flux through the coil (2.66). [21]

$$\vec{J}_M(\vec{r}, t) = \vec{\nabla} \times \vec{M}(\vec{r}, t) \quad (2.64)$$

$$\vec{A}(\vec{r}) = \frac{\mu_0}{4\pi} \int d^3r' \frac{\vec{J}(\vec{r}')}{|\vec{r} - \vec{r}'|} \quad (2.65)$$

$$\Phi = \int \vec{B} \cdot d\vec{S} = \int (\vec{\nabla} \times \vec{A}) \cdot d\vec{S} = \oint d\vec{l} \cdot \vec{A} \quad (2.66)$$

The magnetic field produced in the coil,  $\vec{B}_{rec}$  is described in equation 2.67. We now get a new expression for the flux through the coil, and the induced voltage *emf* is shown in equation 2.69. [21]

$$\vec{B}_{rec}(\vec{r}) = \vec{B}(\vec{r}')/I = \vec{\nabla}' \times \left( \frac{\mu_0}{4\pi} \oint \frac{d\vec{l}}{|\vec{r} - \vec{r}'|} \right) \quad (2.67)$$

$$\Phi(t) = \int d^3r \vec{B}_{rec}(\vec{r}) \cdot \vec{M}(\vec{r}, t) \quad (2.68)$$

$$emf = -\frac{d}{dt} \int d^3r \vec{M}(\vec{r}, t) \cdot \vec{B}_{rec}(\vec{r}) \quad (2.69)$$

### **k-space and gradients, TR, TE and pulse sequence**

After a RF pulse has excited the spin system, the signal from the  $M_0$  disappears before it can be measured. This is due to the  $M_0$  vector spreading out through the x-y plane through transverse magnetization decay, and thus losing its strength. To regain the signal, a new pulse is sent out to refocus the magnetization vector. This pulse has a strength that can tip the nuclei  $180^\circ$ . The time from the first to the second pulse is called Echo Time (TE). The time that passes until a new  $90^\circ$  RF pulse is sent out from the last one is called Repetition Time (TR). [26]

To acquire the image, pixels are sampled into k-space. This is done using gradients, specifically slice, phase and readout gradients. The gradients are added to give localized variations to the main  $\vec{B}_0$  field, allowing us to sample from only a specific area. A Fourier transform converts the pixels in k-space to an image.

### T1-weighted structural imaging using Magnetization-Prepared Rapid Gradient Echo

Magnetization-Prepared Rapid Gradient Echo (MP-RAGE) is an image acquisition technique used in MRI. The technique starts with a magnetization preparation (MP) period that, for T1 images, consists of an inversion pulse followed by a rapid gradient echo (RAGE) sequence to sample the prepared magnetization and ends with a magnetization recovery period. Figure 2.9 shows the sequence diagram for MP-RAGE, which is used for the T1 acquisition in this project. First, a  $180^\circ$  pulse is applied to invert the spin of the slice selected by the slice selection gradient ( $G_S$ ). During the MP period, the T1 relaxation starts. An  $8^\circ$  pulse and the  $G_S$  is applied to push the magnetization into the  $M_{xy}$  plane. For each repetition of the  $8^\circ$  pulse, the  $G_S$  is adjusted slightly to image all slices in the volume. The phase encoding gradient ( $G_P$ ) and readout gradient ( $G_R$ ) are applied to make a single slice in k-space. [26] MP-RAGE is the method used to acquire structural images in this project.

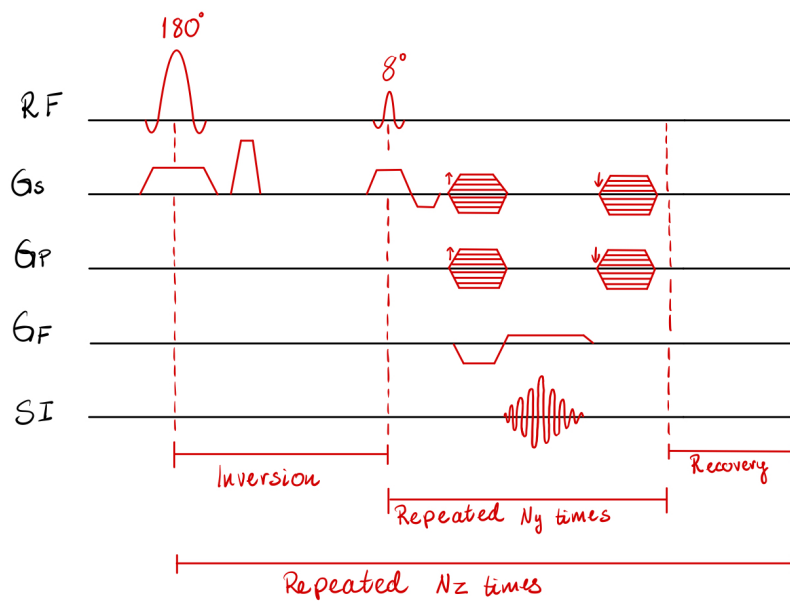


**Figure 2.9:** Sequence diagram for the MP RAGE sequence. Modified figure from [26]

### 2.2.2 Perfusion through Arterial Spin Labeling

Brain perfusion is a measurement of Cerebral Blood Flow (CBF), which refers to the delivery of blood volume to a defined amount of tissue per unit of time. Perfusion is measured in mL blood / 100 g tissue / minute. [28]. CBF typically ranges from 50-70 mL / 100 g / min in cortical GM and about 20 mL / 100 g / min in White Matter (WM) [29]. Arterial Spin Labeling (ASL) is an MRI-based method that takes advantage of the arterial blood water as a tracer to quantify absolute CBF [28].

### 2.2.3 Perfusion Physiology

The brain cells are dependent on a stable blood supply to maintain normal function. The brain receives around 750 mL of blood per minute, or around 15% of the blood pumped by the heart every minute. If the arterial blood pressure falls, the circulatory system will keep the blood supply to the brain stable to prevent any damage to the brain stem. The total blood supply does not change depending on activity levels, but regional supply will vary. Moving your fingers will increase blood supply to the motor cortex, while reading will increase supply to the occipital lobe, which is important for visual perception, and the temporal lobe and the frontal lobe, which are important for language. [30]

The blood transports oxygen to the cells, providing a source of energy. The blood flow to these areas increases because the more active regions use more oxygen than the less active regions. The blood consists of over 50% plasma, which again consists of around 92% water. Using this water as a tracer allows for the study of activity in different regions. [30]

### 2.2.4 Perfusion Imaging

#### **The principles of ASL**

ASL is an MRI technique used to measure perfusion. Compared to other MRI-based perfusion quantification methods, ASL has some advantages. As opposed to gadolinium-contrast-based dynamic-susceptibility contrast (DSC) or dynamic contrast-enhanced MRI (DCE), ASL does not require an exogenous tracer, and the labeled water is not confined to intravascular space. This allows for immediate repetition and avoids pharmacological side effects. [29]

#### **Label and control**

To create a CBF map, two images are acquired: one labeled image and one control image. Both images are acquired using the same readout method, and subtracting the labeled image from the control image gives a perfusion image, but without units [29]. Figure 2.10 shows a simplified illustration of the labeling and image subtraction.

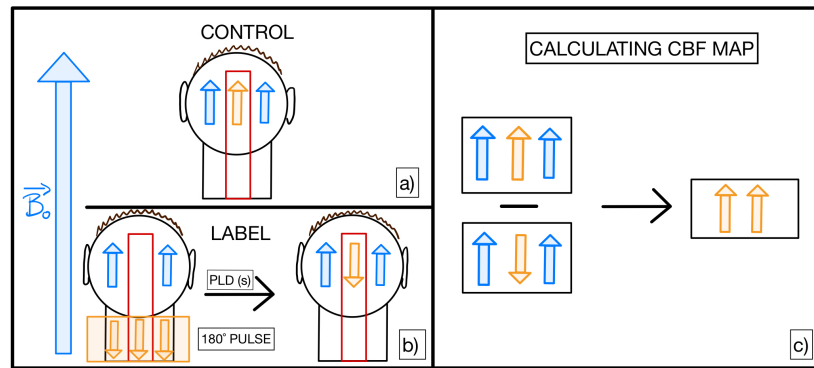


**Figure 2.10:** Simple illustration of the principles of ASL: labeling the water and subtracting the label from the control image. The labeled image (b) is subtracted from the control image (a) to create the perfusion map (c). Modified figure from [28]

To get the units as mL / 100 g / min, an additional image, known as the  $M_0$  image, must be obtained. As explained previously,  $M_0$  is the initial tissue magnetization and contains information about the basic tissue magnetization. It is used to translate how high a signal is for a certain amount of protons. The relative difference between the control and label image is typically 1-2% of  $M_0$ , which results in a poor Signal-to-noise ratio (SNR). To improve the SNR and the final result, several label-control pairs are acquired. [29]

### pASL/cASL/pcASL

The labeled image can be created in one of three ways, using Pulsed ASL (pASL), Continuous ASL (cASL) or Pseudo-Continuous ASL (pcASL). All three methods follow the same set of principles but have slightly different execution. First, a 180-degree RF pulse is applied to a specific area, inverting the magnetization for the hydrogen atoms in the blood water. The water will then travel through the vascular system in the brain, and be delivered to the tissue. After a set time, called the Post-Labeling Delay (PLD) or Inversion Time (TI), an image is acquired. When using pASL a short pulse is applied to a larger slice, inverting the hydrogen atoms inside this volume. pASL has low energy deposition to the tissue, but low SNR. When using cASL a longer pulse is applied to a plane, continuously inverting the hydrogen atoms that pass through. cASL has higher SNR, but higher energy deposition. pcASL is the labeling method that is used the most of these three. Instead of applying a continuous pulse, a series of rapid short pulses is

applied. This way, we get a high SNR but low energy deposition to the tissue. [29]

### Quantifying CBF

To quantify the perfusion in mL / 100g / minute, two assumptions are made. The first assumption is that in the control image, the blood water is fully relaxed, and is described by the  $M_0$ . For arterial blood, it is called  $M_{0a}$ . The magnetization of the blood-water after the inversion pulse in the labeled image is described by equation 2.70. The difference in signal between these images is described by equation 2.71, where  $TI$  is the time delay and CBF is for simplicity called  $f$  in the following equations. [28].

$$-M_{0a} \cdot f \cdot TI \quad (2.70)$$

$$\Delta M = 2M_{0a} \cdot f \cdot TI \quad (2.71)$$

The labeled water is not stationary, and flow effects must be taken into consideration. Labeled water arrives through the arteries, leaves through the veins, and the hydrogen atoms decay back through T1 decay to their original lower state. Because of this, a modification of the Bloch equation called the  $T1$  quantification model is introduced, see equation 2.72. Here,  $M$ ,  $M_a$  and  $M_v$  are the magnetizations of the tissue, arterial and venous blood, respectively. [28]

$$\frac{dM(t)}{dt} = \frac{M_0 - M(t)}{T1} + fM_a(t) - fM_v(t) \quad (2.72)$$

The blood flow adds ( $fM_0adt$ ) and subtracts ( $fM_vdt$ ) magnetization to the area. The relationship between the magnetization of blood and tissue is defined by equation 2.73.  $\lambda$  is the volume distribution between tissue and blood. [28]

$$M_v(t) = \frac{M(t)}{\lambda} \quad (2.73)$$

The second assumption to quantify the perfusion in mL / 100g / minute, is that the magnetization of fully relaxed blood during equilibrium  $M_{0a}$  is equal to  $M_{0a}/\lambda$ . The magnetization change due to the flow can then be described by equation 2.74. [28]



$$dM(flow) = fM_0a(t) - fMv(t) = (M_0 - M(t))\frac{f dt}{\lambda} \quad (2.74)$$

This result can be included in equation 2.72 to give equation 2.75. [28]

$$\frac{dM(t)}{dt} = \frac{M_0 - M(t)}{T1} + \frac{f}{\lambda}(M_0 - M(t)) \quad (2.75)$$

The labelled blood flow also leads to a time-dependent decrease in the magnetization  $M_0$  by an apparent time constant  $T1_{app}$ . The magnitude of  $T1_{app}$  depends on the T1 relaxation time of both tissue and blood and is given by equation 2.76. [28]

$$\frac{1}{T1_{app}} = \frac{1}{T1} + \frac{1}{\lambda} \quad (2.76)$$

The model has so far not included any systematic errors like variable transit time and blood-water exchange between capillaries and tissue and how it affects the T1 relaxation time. To make a more generalized model, the general kinetic model is used as base. It considers the difference signal as the concentration, or magnetization, of the blood-water that remains in the tissue after a time  $t$ . The amount of magnetization left at time  $t$  depends on delivery by arterial flow, removal by venous flow and longitudinal magnetization. Three functions need to be defined.  $C(t)$  is the delivery function and describes how much magnetization arrives at time  $t$ .  $R(t)$  is the residue function and is the fraction of remaining blood water at time  $t$ .  $M(t)$  is the magnetization relaxation function and is the fraction of remaining longitudinal magnetization in the remaining blood-water at time  $t$ . Systematic errors can be accounted for by modifying these functions appropriately. Some assumptions must be made to do this: [28]

Assumption 1: Before the initial transit time  $\Delta t$  no labeled blood-water has arrived. Then after  $\Delta t$  it continues to arrive for as long as the bolus duration ( $\Delta t + t$ ). The delivery function can be defined as equation 2.77. Part 1 of equation 2.77 is valid for pASL, and part 2 is valid for cASL. [28]

$$\begin{aligned} C(t) &= \exp(-t/T1b) \\ C(t) &= \exp(-\Delta t/T1b) \end{aligned} \quad (2.77)$$

Assumption 2: The kinetics of the water exchange between tissue and blood follow the rules of "single compartment kinetics". This means that the water exchanges rapidly between any sub-compartments between these tissues, which leads to a constant concentration within a tissue as a function of time. If assuming a constant concentration ratio between tissue and venous area, which is equal to the volume distribution between tissue and blood  $\lambda$ , the residue function can be described by equation 2.78. [28]

$$r(t) = \exp(-ft/\lambda) \quad (2.78)$$

Assumption 3: Immediately after the tagged blood-water arrives at the voxel, it is completely removed from the vascular space to the tissue. The tagging will therefore decay with the T1 relaxation of the tissue. The magnetization relaxation function can be defined as equation 2.79. [28]

$$m(t) = \exp(-t/T1) \quad (2.79)$$

The general kinetic model is collected in equations 2.80 and 2.81. Here,  $\Delta t$  is the initial arrival time of the labeled blood,  $\tau$  is the duration of the arterial bolus. [28]

$$C(t) = \begin{cases} 0 & 0 < t < \Delta t \\ \exp(-t/T1b) & \text{pASL} \\ \exp(-\Delta t/T1b) & \text{cASL} \\ 0 & \end{cases} \quad (2.80)$$

$$\begin{aligned} r(t) &= \exp(-ft/\lambda) \\ m(t) &= \exp(-t/T1) \end{aligned} \quad (2.81)$$

An alternative equation for the delivery function  $C(t)$  can now be introduced. For any agent that is not metabolized, the tissue concentration curve  $Ct(t)$  is the convolution (\*) of the delivery function  $C(t)$  and the local impulse function  $R(t)$  which contains both  $r(t)$  and  $m(t)$ , as shown

in equation 2.82. [28]

$$Ct(t) = fC(t) * R(t) \quad (2.82)$$

Right after the inversion pulse, the arterial magnetization difference is  $\Delta M = 2M_0a$ . This is delivered to the voxel as  $2M_0afC(t)$ . If we add this to equation 2.82, we get a measure of cerebral perfusion in equation 2.83. The brackets refer to an integral of the time dimension over the bolus duration. [28]

$$\Delta M(t) = 2M_0afC(t) * [r(t)m(t)] \quad (2.83)$$

By combining equation 2.80, 2.81 and 2.83, it gives a solution for pASL in equation 2.84.  $\alpha$  is the inversion efficiency,  $R1a$  is the blood relaxation rate,  $R1app$  is the apparent tissue relaxation rate, and  $\delta R = R1a - R1app$  [28].

$$\Delta M(t) = \begin{cases} 0 & 0 < t < \Delta t \\ \frac{-2M_0a \cdot \alpha \cdot f}{\delta R} e^{-R1a \cdot t} \left( 1 - e^{-\delta R(t-\Delta t)} \right) & \Delta t < t < \Delta t + \tau \\ \frac{-2M_0a \cdot \alpha \cdot f}{\delta R} e^{-R1a \cdot \Delta t} \left( 1 - e^{\delta R(t-\Delta t)} \right) \cdot e^{R1app(t-(\Delta t+\tau))} & \Delta t + \tau < t \end{cases} \quad (2.84)$$

The formula for quantifying CBF in each voxel is given by equation 2.85. The factor of 6000 is used to convert from mL / g / s to mL / 100 g / min. For pcASL  $\alpha = 0.85$ .  $T1a$  is the blood relaxation time, approximated to 1650ms at 3T.  $SI_{control}$  and  $SI_{label}$  is the average signal intensity in the voxel in the control and labeling image, while  $SIPD$  is the measured value of proton density. [28]

$$\frac{6000 \cdot \lambda \cdot (SI_{control} - SI_{label} \cdot e^{PLD/T1a})}{2 \cdot \alpha \cdot T1a \cdot SIPD \cdot (1 - e^{-\tau/T1a})} [mL/100g/min] \quad (2.85)$$

### Single-PLD v.s. Multi-PLD

To acquire the labeled image, a single or multiple PLDs can be used. Multi-PLD ASL provides more information about the temporal aspect of the labeled blood arrival but is more time-

consuming. [29]

### **The White paper standard**

White paper is a standard for ASL imaging for clinical applications by the International Society for Magnetic Resonance in Medicine (ISMRM) Perfusion Study Group and the European 'ASL in Dementia' consortium. The recommendations include using a 3T system, using pcASL for labeling, and readout using a 3D acquisition method. [31]

### **CBF variations**

When studying a physiological property like CBF, it is important to know its natural day-to-day variations. An article from 2018 [32] found that regional CBF values increased from morning to night, and then decreased again after a night of sleep. An article from 2018 [33] looked at perfusion variability among healthy subjects in studies published between 1952 and August 2016 and found that factors like caffeine, aging and blood gases were consistent in affecting brain perfusion across different studies.

## **2.3 Electromagnetic stimulation**

### **2.3.1 Electroconvulsive therapy**

In ECT a controlled seizure is induced by applying a focused amount of electricity to the brain. The seizure lasts for about 20-90 seconds and is believed to be largely responsible for the benefit of ECT on MDD and other mental disorders. The patients receive a muscle relaxant to prevent damage to muscles and bones due to the convulsion. The electrical stimulus immediately causes unconsciousness and is not painful, but to prevent awareness and any memory of muscle paralysis, the patient also receives anesthetic narcosis. There are four main electrode placements used in ECT: Bitemporal (BT), Right Unilateral (RUL), Bifrontal (BF) and Left Anterior Right Temporal (LART). For the BT placement, the electrodes are placed on each temple just behind the forehead [34]. This placement has the best efficacy compared to the other placements, but it is considered to cause more cognitive impairment [35]. For RUL, one electrode is placed on the right temple, and the other just right of the vertex on top of the head [34]. It is one of the most used placements in contemporary ECT [35]. In BF, each electrode is placed about 2.5 cm in front of the bitemporal (just above the eyebrows). For LART one electrode is placed on the forehead about 5.0cm in front of the bitemporal, and the other is placed on the right tem-

ple. The typical dose given is 900 mA [34]. The electrical impulse from the electrodes traverses through the intermediate tissue, stimulating the neurons by altering their electrical environment and ion concentrations. Groups of depolarized neurons then fire simultaneously, inducing a seizure. [36].

ICD is an international classification of diagnoses. ICD-10 is the tenth edition which is the one currently in use in Norway [37]. Several ICD-10 codes qualify for ECT or TMS treatment. They include bipolar disorder (F31), depressive episodes (F32) and recurrent depressive disorder (F33) [38]. The Montgomery-Åsberg Depression Rating Scale (MADRS) is a diagnostic tool to assess the severity of depressive symptoms [39]. It is a questionnaire covering ten symptoms, with each symptom yielding a score between 0 and 6. More than 20 points indicate moderate depression, while more than 35 points indicate severe depression [40].

The electricity is given as brief squared pulses, and the pulse width influences the efficacy and side effects of the treatment. A typical pulse width is around 0.5-2 ms, and a typical stimulus frequency is 30 Hz. [34]. Figure 2.11 shows a simple illustration of a brief pulse stimulus. Because the instrument delivers two pulses per wavelength, one with positive amplitude and one with negative, a frequency of 30 Hz corresponds to 60 pulses per second. A frequency of around 30 Hz is often more desirable than higher frequencies, as it shows more efficiency, but the frequency is more important here. [34]

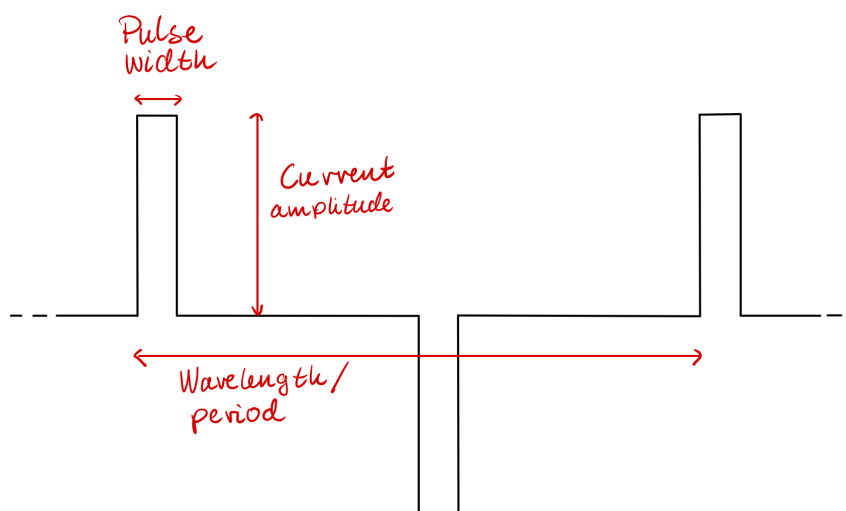


*Figure 2.11: Simple illustration of a brief pulse stimulus.*

### 2.3.2 Transcranial magnetic stimulation

TMS is another method that delivers an electrical stimulus to the brain through the scalp. As opposed to ECT; the TMS treatment is delivered while the patient is conscious. TMS using a single pulse is generally used to explore brain function, while repetitive TMS (rTMS) is used to change brain activity for a longer period after the treatment [13]. TMS uses Faraday's principle of electromagnetic induction to stimulate neurons. By running a current through a coil, a current is induced in the nearby surface, which in the case of TMS is the brain tissue. If the current through the TMS coil is large enough, and the magnetic field changes rapidly enough, the induced electric field in the brain tissue will cause the neurons to fire [14]. Figure 2.12 shows how the current in the TMS coil leads to an induced current in the brain tissue.

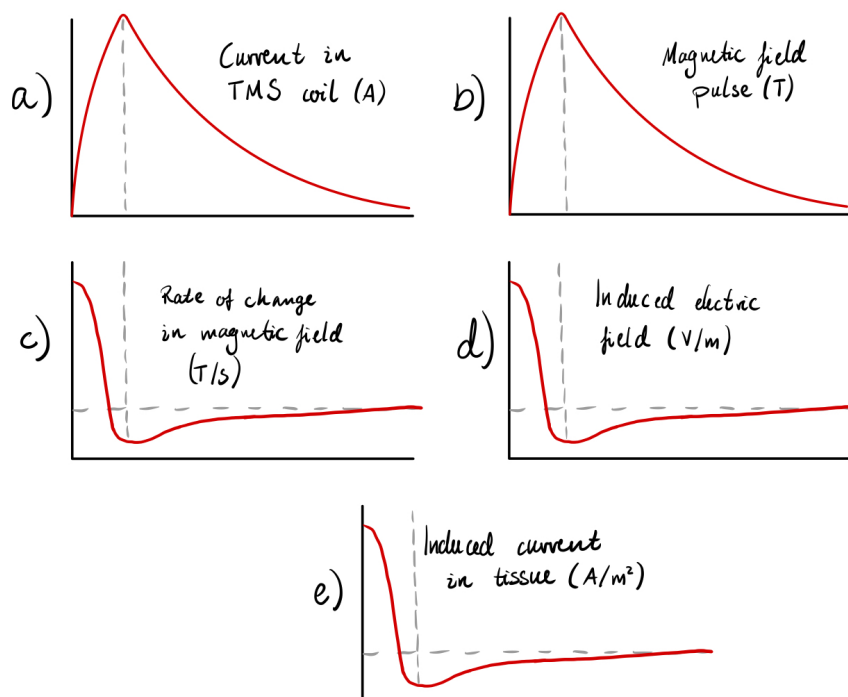


**Figure 2.12:** The working mechanisms of TMS. The current in the TMS coil (a) induces a magnetic field (b). The field has a rate of change (c), which induces an electric field (d) and current (e) in the tissue. Modified figure from [14]

### 2.3.3 Application in mental disorders

#### The origins

ECT has been used as a treatment for several psychiatric conditions since its first introduction in 1938 by Ugo Cerletti and Lucio Bini [41] [42], but the idea to induce seizures to treat mental illness can be traced back to the 1500s when camphor oil was used to induce seizures [16]. The discovery of electricity-induced seizures was a medical revolution and has since helped

millions of mentally ill patients [41]. In the late 1920s a researcher from the University of Budapest, Meduna, observed that glial cells occupied the spaces left by lost neurons in patients with epilepsy. In 1931 his colleague Hechst described a reduction of glial cells in the brain of schizophrenia patients, indicating an antagonism between epilepsy and schizophrenia. In 1934 Meduna conducted the first human experiments using camphor to induce seizures to treat schizophrenia, and in the two following years over 100 patients were treated and over half significantly improved. Although the camphor was effective, the seizures were unpredictable, and the time between injection and seizure was stressful for the patients. This led Cerletti and his assistant Bini to search for alternative seizure inductions. Safe parameters of electric stimulus were decided through animal studies, and the first electric stimulus was tested on a patient in 1938. The patient recovered after 11 treatments. [42]

TMS by a single electrical pulse using a probe was first used in animal studies in the 20th century. In 1980, the motor cortex was successfully stimulated in humans through Transcranial Electrical Stimulation (TES) by two electrodes. The procedure was uncomfortable for the patients, and only a fraction of the current was thought to enter the motor cortex, while the rest was contracting the scalp muscles and inducing local pain. In 1985 TES was replaced with TMS. [13].

### **How do we think it works?**

Meduna's hypothesis about the antagonism between epilepsy and schizophrenia was never confirmed, and the working mechanism is not yet known, but there are several theories. One theory explains the effect by referring to the effect on the neurotransmitters like serotonin and dopamine. Another theory treats depression like an inflammation, as ECT influences cytokines and therefore treats the inflammation. Some of the most promising theories involve ECT-induced changes in brain plasticity. [42]. The generalized seizure theory claims that the therapeutic effect of ECT is dependent on inducing seizures. The neuroendocrine-diencephalic theory claims that ECT restores a neuroendocrine dysfunction in hormones like cortisol that is associated with severe depression. A combined anatomical-ictal theory claims that seizure activity in the limbic system induces neurotrophic effects which are important for ECT efficacy. The neurotrophic effects include volume increases of the hippocampus in humans and hippocampal neurogenesis in animals. [43]

### 2.3.4 Biological effects and side effects

#### Memory loss and other cognitive effects

ECT treatment may affect several domains of cognitive function. A meta-analysis from 2020 [44] looked at several studies of cognitive side effects to create guidelines to aid clinicians and inform patients. One meta-analysis [45] discussed impairment in new learning, but the scores returned to baseline 14 days after the ECT treatment. Side effects also included deficits in autobiographical memory. The meta-analysis also investigated factors that may increase the risk of side effects. ECT treatment parameters, like pulse width and electrode placement, and individual factors may affect the risk of cognitive effects. While the efficacy is higher for BL than RUL electrode placement, there are also more severe side effects.

#### Hippocampal volume

Hippocampal volume change is a physiological effect commonly observed after treatment with ECT [5]. The hippocampus plays an essential part in learning and memory [46] and experiences a volume reduction during major depression [17]. Increased hippocampal volume can occur after extensive learning [16].

## 2.4 Current knowledge

#### Depression and volume change

A lot of research has been conducted on ECT and volume change. Patients with depression have been shown to have a reduced volume in the hippocampus [47][48] and amygdala [48], and the effect is more prominent with patients who have recurrent MDD [47]. Patients with a history of recurrent depression who are currently in remission also have lower hippocampal volumes than healthy controls. [49]

#### ECT and volume change

Many volumetric studies focus on structures like the hippocampus and amygdala and find a volumetric increase in these areas [15] [50]. The increased volume is most often found in the right hemisphere, which is consistent with the RUL electrode placement and the distribution of the electric field through the brain [17]. A Global ECT-MRI Research Collaboration (GEMRIC) study from 2020 found a volume increase in 79 of 84 GM ROIs [18].

A GEMRIC study from 2019 used electric field modeling in patients with depression who re-



ceived ECT to determine the relationship between electric field and volume change and antidepressant response. While most ROIs showed a volumetric increase, only the left amygdala and left hippocampus had a strong relationship between electric field and volume change after correcting for variables like age and number of treatments. The study showed no relation between electric field or volume change with antidepressant response.[5]

A master's thesis from the University of Bergen studied the volume change in the hippocampus and surrounding regions. It studied the relationship between volume change and electric field strength in the hippocampus, amygdala, thalamus, and caudate. The thesis found that the left hippocampus and left amygdala had a statistically significant relationship between electric field strength and volume change, and the relations were generally stronger in the left hemisphere than in the right hemisphere. [51]

### **Bipolar Disorder**

A study from 2017 evaluated the short-term outcome of ECT on 522 patients with BD and found that 68.8% responded to the treatment, and the response rates were high for depressive and manic moods, as well as for mixed and catatonic moods [11]. Another study from 2012 found that patients with BD had smaller hippocampal volumes compared to healthy controls, and they also showed impaired verbal memory [52].

### **TMS**

Volume changes after TMS treatment are less explored than volume changes after ECT. An article from 2020 [4] studied volume changes in the hippocampus and amygdala. The study found that gender significantly influenced volume changes in the amygdala. However, no other significant changes over time or between groups for the amygdala or hippocampus were found. A study from 2023 [6] looked at brain volumes in rats who had disrupted neurodevelopmental processes and human adolescents with early-onset mental disorders. The study of the adolescents found a significant increase in hippocampal volume after TMS treatment compared to the baseline, and the volumetric changes had a significant connection to improvement.

### **Perfusion**

A meta-analysis from 2016 [36] looked at neurobiological mechanisms for ECT, among them brain perfusion. One of the studies found that global CBF increased during the treatment and then returned to the pre-ECT baseline 10 to 30 minutes later. [53]. Other studies measured perfusion after complete treatment using Positron Emission Tomography (PET) or Single-Photon

Emission Computed Tomography (SPECT). One study found that ECT patients had lower baseline metabolism in the superior frontal gyrus and higher baseline metabolism in the inferior temporal gyri than healthy controls. The changes persisted after the ECT treatment. The study also showed an increased metabolism in the right medial temporal structures, including the amygdala. [54] Another study found decreased metabolism in the left temporal cortex [55].

## **2.5 Thesis motivation and aim**

This thesis aims to investigate whether volumetric changes in selected brain structures occur as a response to ECT and TMS treatment. The thesis will then investigate if perfusion accompanies the volume changes.

If changes in perfusion accompany the volumetric changes, it might explain why the increases happen and contribute to our understanding of how the treatment works.

In this thesis, the effect of both ECT and TMS on volume change and perfusion will be studied. This may contribute to the understanding of how the electric field strength affects both the volume change and any perfusion changes, as the field strength from the TMS treatment is much lower than the field strength from the ECT treatment.

The analysis will be performed on data in an ongoing clinical trial. This makes the dataset rather small, but it means it can be repeated when the dataset is complete to see if the same results are found.

# Chapter 3

## Methods

### 3.1 Participants

The data was collected following the procedure described in [56].

The dataset consists of 28 participants, of whom 9 received ECT treatment, 10 received TMS treatment, and 9 were healthy controls who only participated in the imaging. The patients receiving ECT or TMS must be over the age of 18, and be referred to the treatment of moderate and severe depression, meeting the criteria for the following ICD-10 diagnoses: [56] F31.3 and F31.4 (bipolar [38]); F32.1 and F32.2 and F32.3 (depressive episode [38]); F33.1 and F33.2 and F33.3 (recurrent depressive episodes [38]) [56]. The symptom intensity must also be verified by a MADRS over 25. Patients who have had ECT or TMS treatment within the last 12 months, are unable to give informed consent or have contradictions to MRI scanning were excluded from the study. The healthy controls are age and sex-matched to the patients, have no history of mental disorder, and were also screened for other medical conditions or drug use [56] Table 3.1 shows the number of participants in each group, the age distribution and the diagnostic categories that are used in this project. One TMS participant was excluded from this project due to not following the scan intervals shown in Figure 3.1.

**Table 3.1:** Information about the study participants across the three groups. *std* = standard deviation, *N* = number of participants.

	Control	ECT	TMS
N (female)	9 (4)	9 (3)	10 (6)
Age (mean $\pm$ std)	44.6 $\pm$ 16.5	42.0 $\pm$ 10.7	37.9 $\pm$ 10.7
Diagnostic category	N/A	F32.2, F33.1, F33.2, F33.3	F31.3 F31.4, F32.1, F32.2, F33.1, F33.2

## 3.2 Treatment

### 3.2.1 ECT

The ECT treatment was administered three times a week until remission or for a maximum of 18 sessions. Right unilateral positioning was used unless clinical indication suggested bilateral positioning would benefit the patient more. The current was administered using a Thymatron System IV (Somatic Inc). The machine produces a brief, square wave at a constant 900mA current, with an initial stimulus pulse set to 0.5ms. The stimulus dose was calculated based on an age-based method. [56]

### 3.2.2 TMS

The TMS treatment was administered five times a week for six weeks using a TMS stimulator with a figure-8 coil. First, the motor threshold for the right-hand muscles is determined[56], which is at the left side of the head as the left hemisphere controls the right side of the body [30]. Then, the coil is placed 5cm anterior to the motor threshold. Each treatment session produced 1500 TMS pulses, delivered in 15 groups of 100 pulses, with 30s intervals at frequency 10Hz, totaling to 9min 30s of treatment per treatment session. [56]

## 3.3 MRI acquisition

The participants received between three and five MRI scans, at 1-2 hours before, 1-2 hours after, 15 days after, 3-8 weeks after and 7-8 months after the first treatment [56]. The MRIs of interest in this thesis are the T1 and ASL sequences. The T1 images were acquired using the sagittal 3D MPRAGE with voxel size 1 mm  $\times$  1 mm  $\times$  1 mm, TE = 3.1 ms TR = 7.4 ms, inversion time = 1060 ms, time between consecutive inversion = 2798 ms, FOV = 256  $\times$  256 ms,  $\alpha$  = 8°, sagittal acquisition with 208 slices. The ASL images were acquired using 3D ASL with voxel

size  $1.875 \text{ mm} \times 1.875 \text{ mm} \times 4 \text{ mm}$ , TE = 10.5 ms, TR = 4888 ms, and the labeling was done using pcASL.

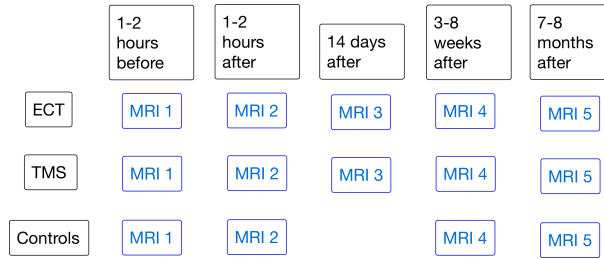


**Figure 3.1:** A flowchart showing the MRI acquisitions for the different groups. The timestamps are the time before or after the first treatment. All participants were scanned at 08:00, except at scan 2, performed at 12:00.

### 3.4 MRI analysis

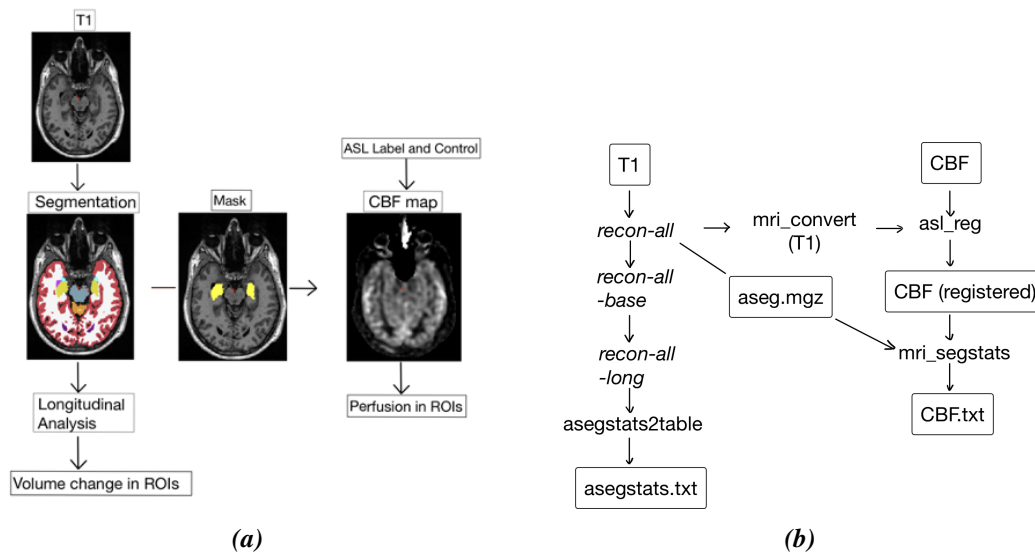


**Figure 3.2:** An illustration of the data processing. The T1 images were segmented using FreeSurfer, and the masks were used on the CBF maps to calculate the perfusion in the areas. (a) Sample images to show the analysis using FreeSurfer and FSL BASIL. The MRI machine calculates the CBF map based on label and control. The masks are of the left and right hippocampus. (b) The FreeSurfer and FSL BASIL commands used to analyze the images. The entries with borders are images and files, while the rest are commands.

The MRI images were processed using FreeSurfer (v.7.4.1) [8] and FSL BASIL (v.6.0.7.7 and v.4.0.4, respectively) [9]. FreeSurfer is a software for processing, analyzing, and visualizing human brain MR images. FSL BASIL is a tool used to quantify the perfusion of ASL data. Figure 3.2 shows FreeSurfer and FSL BASIL commands on the dataset and sample images. A pipeline was established to analyze the images. A link to the scripts can be found in Appendix B.

### 3.4.1 FreeSurfer segmentation and longitudinal analysis

FreeSurfer was used to perform segmentation and longitudinal analysis. FreeSurfer's command *recon-all* [57] was used to do the segmentation. This command performs all the FreeSurfer commands for processing, analysis and segmentation. The function takes two arguments: *-i input* which is the NIFTI or DICOM input files, and *-s subjid* which will be the name of the folder where the results are stored. The use of the function is displayed in Listing 3.1. The analysis is performed on scan 1 for one participant in the listing. The `\` is used for separating the command over several lines.

*Listing 3.1: Using recon -all on the T1 NIFTI image on scan 1 for one participant*

```
recon-all \
-i /nifti/FXXXXX_1/T1.nii \
-s /recon_results/FXXXXX_1 \
-all
```

#### Base

The first step of the longitudinal analysis is to create a template base that is unbiased to any scan in the longitudinal series [58]. When processing longitudinal data, there is a risk of processing bias. This can happen when a single scan is considered as the baseline, or base, of the processing. Individual differences in that scan will plant themselves through the processing. Therefore, a template base is created in which all the scans in the series are treated as equal contributors. The images are iteratively registered into a median image. The processing can then be done in a spatially normalized voxel space across time, which reduces variability. [59] Creating the base is done using the *recon -all* command with the flag *-base*. The command takes all the scans as input and creates the base. [58] Listing 3.2 shows the creation of the base for a set of 4 scans for one participant. The resulting base will be saved in the folder *FXXXXX\_1\_base*.

*Listing 3.2: Using recon -all with flag -base to create unbiased base to do longitudinal processing for a participant with 4 scans*

```
recon-all \
-base recon_results/FXXXXX_base \
-tp recon_results/FXXXXX_1 \
-tp recon_results/FXXXXX_2 \
-tp recon_results/FXXXXX_3 \
```

```
-tp recon_results/FXXXXX_4 \  
-all
```

### Long

The last step of the longitudinal processing was done using the *recon -all* command with the flag *-long* [58]. Listing 3.3 shows the command for the longitudinal analysis for participant *FXXXXX* at scan 1, using the base *FXXXXX\_base*. The analysis will be stored in the folder *FXXXXX\_1.long.FXXXXX\_base*.

**Listing 3.3:** Using *recon -all* with flag *-long* to do the longitudinal analysis for participant *FXXXXX* at scan 1 using the base *FXXXXX\_base*

```
recon -all \  
-long recon_results/FXXXXX_1 \  
recon_results/FXXXXX_base \  
-all
```

### 3.4.2 Quantification of volumetric changes

After doing FreeSurfers longitudinal analysis, the command *asegstats2table* was used to extract the volumetric information across all scans for the ROIs of all participants. The command *asegstats2table* is the approach recommended by FreeSurfer for analyzing the longitudinal data. It uses the file *aseg.stats* from each longitudinal analysis and saves the volumetric value in a table for easy access [60]. *asegstats2table* takes the input arguments *-i* and creates the file *asegstats.txt* [61]. A snippet of the code used to extract the volumetric values is shown in Listing 3.4.

**Listing 3.4:** Using *asegstats2table* to create a table with all volumetric info for all subjects for all scans

```
asegstats2table \  
-i recon_results/FXXXXX_1.long.FXXXXX_base/stats/aseg.stats \  
.  
.  
.  
recon_results/FYYYYY_5.long.FYYYYY_base/stats/aseg.stats \  
--meas volume \  

```

```
--tablefile asegstats.txt
```

### 3.4.3 Quantification of perfusion changes

To calculate the CBF values in the ROIs, the CBF maps had to be registered to the T1-weighted images. The CBF images are of lower resolution, and registration makes sure that the CBF value in an area corresponds to the anatomical placement in the T1-weighted image. The T1 images from the FreeSurfer output were used, to make sure the FreeSurfer volumetric segmentation and perfusion quantification were as comparable as possible. They are of type *.mgz*, and must first be converted to NIFTI. This conversion is shown in Listing 3.5. The images were then registered using *asl\_reg* from the FSL BASIL library. The command takes arguments *-i* as the CBF map to be registered, *-o* as where to put the registration, and *-s* is the T1-weighted image the CBF map is registered onto. The code is shown in Listing 3.6.

*Listing 3.5: Converting the T1-weighted images from the FreeSurfer recon-all output from .mgz to NIFTI for the registration*

```
mri_convert recon_results/FXXXXX_1/mri/T1.mgz \
registration/rawdata/T1_FXXXXX_1.nii
```

*Listing 3.6: Registration of the CBF map onto the T1-weighted image from the FreeSurfer output*

```
asl_reg -i nifti/FXXXXX_1/CBF.nii \
-o registration/FXXXXX_1 \
-s registration/rawdata/T1_FXXXXX_1.nii
```

To calculate the perfusion, the command *mri\_segstats* was used. The command takes the arguments *- -seg* which is the segmented volume, *- -i* which is the registered CBF map, *- -ctab* specifies the look-up-table for the labels, and the result is stored in the file specified by the flag *- -sum*. Listing 3.7 shows the use of *mri\_segstats* for one subject at scan 1.

*Listing 3.7: Calculating the CBF value of all segmentations from the FreeSurfer analysis*

```
mri_segstats \
--seg recon_results/FXXXXX_1/mri/aseg.mgz \
--i registration/FXXXXX_1/asl2struct.nii.gz \
--ctab $FREESURFER_HOME/FreeSurferColorLUT.txt \
--sum CBF_calc/FXXXXX/CBF_1.txt
```



## 3.5 Statistical analysis

The statistical analysis is done using Python. The Seaborn library [62], which is based on Matplotlib [63], was used for plotting the figures, while SciPy [64] was used for the statistical analysis. The pandas [65] library was used to create the data frames, and NumPy [66] for the data handling and editing. A link to the scripts can be found in Appendix B.

### Hypothesis-testing

A statistical hypothesis is a claim about the value of a single, several or the distribution of several parameters. In a hypothesis testing scenario, two contradictory hypotheses are considered. One of the claims called the null hypothesis ( $H_0$ ), is initially assumed to be true. The initial claim is rejected if the data gives strong evidence that the alternative hypothesis ( $H_a$ ) is true. [67]

A test is performed on the data to decide whether or not to reject  $H_0$ . The test consists of a test statistic, which is a function of the sample data, and a rejection region, which is the values of the test statistics that lead to a rejected  $H_0$ . Rejecting  $H_0$  when it is true is a Type I error, while not rejecting  $H_0$  when it is false is a Type II error. [67]

### t-test

The Student's t-test checks if the difference between two groups is statistically significant [68]. Two different methods are used to calculate the t-value in this project: the two-sample t-test for independent samples and the dependent t-test for paired samples.

The dependent t-test is used to calculate the t-value and p-value for the same group between two different scans [68]. Equation 3.1 shows the formula used by SciPy to calculate the t-value [69][68].  $\bar{X}$  is the mean of the difference between the pairs  $a$  and  $b$ , and  $SE$  is the standard error of the difference between the pairs. Listing 3.8 shows the SciPy command used to calculate the t-value.

$$t = \frac{\bar{X}}{SE} = \frac{1/n(\sum_i^n a_i - b_i)}{1/\sqrt{n}\sqrt{\frac{1}{n-1}\sum_i^n ((a_i - b_i) - \bar{X})^2}} \quad (3.1)$$

**Listing 3.8:** The Scipy command used to calculate t-value between the scans.

```
scipy.stats.ttest_rel(scan_4, scan_1)
```

The two-sample t-test for independent samples, also called Welch's t-test [70], is used to cal-

culate the t-values and p-values between the different groups. The test is used when the two groups have different variances [71]. Equation 3.2 shows the formula used to calculate the t-statistic.  $\bar{X}_i$  is the mean of group  $i$ ,  $s_i^2$  is the variance of group  $i$ , and  $n_i$  is the sample size of group  $i$ . Listing 3.9 shows the SciPy command used to calculate the t-value.

$$t = \frac{\bar{X}_1 - \bar{X}_2}{\sqrt{\frac{s_1^2}{n_1} + \frac{s_2^2}{n_2}}} \quad (3.2)$$

**Listing 3.9:** *The Scipy command used to calculate t-value between the groups.*

```
scipy.stats.ttest_ind(group, control, equal_var=False)
```

### p-value

The p-value is a probability measure and gives the probability of obtaining the same result given that the hypothesis  $H_0$  is true. If the p-value is low, the  $H_0$  can be rejected [67]. In this project, the p-value is also calculated in the student's t-test, and a significance level of  $p < 0.05$  is used as a requirement to reject  $H_0$ . The p-values were calculated using t-tests and were outputs from the SciPy commands in Listings 3.8 and 3.9.

Bonferroni-correction [72] is a method used to counteract the so-called multiple comparisons problem [73], which happens when several statistical tests are performed simultaneously. In this project, the Student's t-test is performed for 19 areas simultaneously, increasing the probability of coincidentally finding statistical significance, thus rejecting the null hypothesis (Type I error). To compensate, the required significance level is re-calculated by  $\alpha/m$ , where  $\alpha$  is the original p-value threshold and  $m$  is the number of hypotheses [72]. The new, corrected significance threshold in this project is:

$$p - value = \frac{0.05}{19} = 0.0026 \quad (3.3)$$

### Percentage-plots

The variability between participants in measures of volume and perfusion is often greater than the longitudinal variability of the individual participants. To account for variability across participants, the percent changes in volume and perfusion will be calculated and plotted to visually demonstrate the change over time. This is done by first calculating the mean volume or perfusion for the individual participant and using this as a base for calculating the percent change.

### Laterality Index

The laterality index was calculated in the perfusion analysis to ascertain any changes between the hemispheres. The index was calculated using equation 3.4, where  $L$  is the perfusion in the left hemisphere, and  $R$  is the perfusion in the right hemisphere. A larger laterality index indicates a larger difference between the hemispheres. A positive laterality index indicates more perfusion in the left hemisphere, while a negative laterality index indicates more perfusion in the right hemisphere.

$$LI = \frac{L - R}{L + R} \quad (3.4)$$

# Chapter 4

## Results

In this chapter, the results from the image data analysis are presented. The longitudinal change of volume and perfusion in selected Region Of Interest (ROI) is presented in the form of tables and scatterplots. The plots showing the absolute values of volume and perfusion have different colors and shapes across the participants to show the variation. The plots showing the relative percent volume change have a regression line through scan 1, scan 3 and scan 4 to show the change, while the regression lines in the relative perfusion plots include all timepoints. To calculate the change in percent, the mean value for the participant was calculated and used as the baseline. The regression lines have a 95% confidence interval in a more transparent color. The data are assumed to follow a normal distribution.

## 4.1 Volume change

The following section presents the results of the volumetric analysis. A p-value  $< 0.05$  was selected as the significance threshold. Only the plots of the ROIs with a p-value  $< 0.05$  are included.

### 4.1.1 Normal variation

Table 4.1 shows the mean values and standard deviations for scan 1 as well as the change in percent from scan 1 to scan 4, and the t-value and p-value for the selected volumes in the ROIs for the control group. None of the ROIs show a p-value less than 0.05 and have no statistically significant change from scan 1 to scan 4, which is to be expected from the healthy controls. As there are 3-8 weeks between the scans, these estimates provide information about the normal variation across time.

**Table 4.1:** Mean value, standard deviation, percent change from scan 1 to scan 4 and p-value for the volumes in the ROIs for the control group. WM=White Matter, std=Standard Deviation

Areas	Scan 1 mean $\pm$ std ( $mm^3$ )	Change (%)	t-value	p-value
Left-Hippocampus	4344.3 $\pm$ 541.9	0.4	1.04	0.3378
Right-Hippocampus	4404.7 $\pm$ 556.6	-0.6	-1.47	0.1923
Left-Amygdala	1765.5 $\pm$ 296.0	-1.9	-1.98	0.0954
Right-Amygdala	2040.7 $\pm$ 299.3	-0.8	-0.60	0.5684
Left-Thalamus	7775.2 $\pm$ 1146.5	0.7	1.36	0.2217
Right-Thalamus	7550.1 $\pm$ 1020.7	1.1	2.10	0.0807
Left-Caudate	4052.6 $\pm$ 347.7	-0.3	-0.60	0.5711
Right-Caudate	4208.1 $\pm$ 350.1	-0.3	-0.62	0.5610
Left-Cerebellum-WM	15128.7 $\pm$ 2735.8	0.5	0.35	0.7395
Right-Cerebellum-WM	14190.7 $\pm$ 1980.0	-0.5	-0.91	0.3987
Left-Cerebellum-Cortex	58492.9 $\pm$ 7369.4	-0.5	-1.33	0.2309
Right-Cerebellum-Cortex	59682.8 $\pm$ 7582.9	-0.8	-2.37	0.0554
Left-Pallidum	2109.4 $\pm$ 161.6	0.6	0.74	0.4883
Right-Pallidum	2146.1 $\pm$ 222.4	0.4	0.63	0.5553
Left-Putamen	5543.3 $\pm$ 622.5	0.49	0.55	0.6022
Right-Putamen	5542.1 $\pm$ 525.0	0.1	0.16	0.8799
Left-Accumbens-area	693.7 $\pm$ 109.5	-3.9	-1.05	0.3346
Right-Accumbens-area	697.1 $\pm$ 108.8	-0.9	-0.63	0.5543
Brain-Stem	23244.8 $\pm$ 3037.9	0.5	1.31	0.2384

### 4.1.2 Variation across groups

To assess if there was any difference between the groups before the treatment, the difference in total intracranial volume was studied. Figure 4.1 shows the boxplot of the total volume across the three groups, and table 4.2 gives the mean and standard deviation. Because the mean values of each group are well within the range of the mean  $\pm$  standard deviation, there is no difference between the groups in intracranial volume. This is important to know, as it shows the groups are comparable. If one of the groups had a significantly smaller or larger intracranial volume, it would be wrong to compare the volumes of ROIs between groups, as they are dependent.

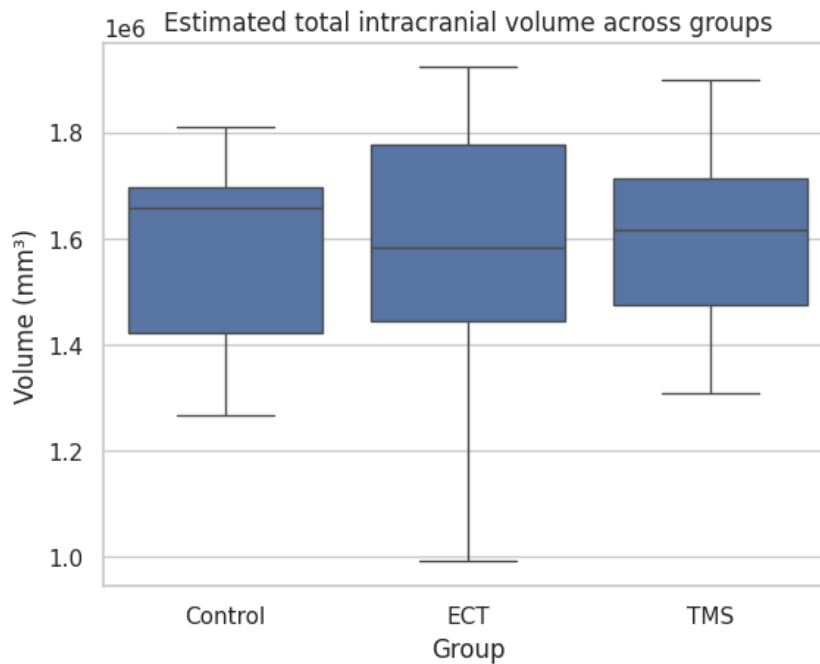


**Figure 4.1:** Boxplot showing the variation of total intracranial volume between the groups

**Table 4.2:** Mean value ( $\text{mm}^3$ ) and standard deviation ( $\text{mm}^3$ ) of the total intracranial volume across the three groups.

Group	Mean value	Standard deviation
Control	1597785.2	180728.6
ECT	1564992.2	269219.9
TMS	1593811.0	179518.0

### 4.1.3 Effect of treatment

It was established that there were no structural differences across the groups. The effect of the different treatments will be presented in this subsection.

#### ECT

Table 4.3 shows the mean values and standard deviations for scan 1 as well as the change in percent from scan 1 to scan 4, and the t-value and p-value for the selected brain structures for the ECT group. The left and right hippocampus, right amygdala and right thalamus showed a statistically significant change from scan 1 to scan 4, with a p-value less than 0.05. In these regions, a relative increase in volumes is seen in the time following the ECT treatment. After a Bonferroni correction, only the right hippocampus and right amygdala have a sufficiently low p-value to be statistically significant ( $p < 0.0026$ ).

**Table 4.3:** Mean value, standard deviation, percent change from scan 1 to scan 4 and p-value for the volumes in the ROIs for the ECT group.

Areas	Scan 1 mean $\pm$ std ( $mm^3$ )	Change (%)	t-value	p-value
<b>Left-Hippocampus</b>	<b>4176.9 <math>\pm</math> 151.9</b>	<b>2.8</b>	<b>4.94</b>	<b>0.0043</b>
<b>Right-Hippocampus</b>	<b>4348.6 <math>\pm</math> 239.5</b>	<b>4.3</b>	<b>11.28</b>	<b>0.0001</b>
Left-Amygdala	1755.3 $\pm$ 158.4	3.7	2.42	0.0601
<b>Right-Amygdala</b>	<b>2105.0 <math>\pm</math> 171.0</b>	<b>4.3</b>	<b>9.74</b>	<b>0.0002</b>
Left-Thalamus	7890.2 $\pm$ 414.8	0.1	0.14	0.8961
<b>Right-Thalamus</b>	<b>7567.6 <math>\pm</math> 406.6</b>	<b>1.8</b>	<b>3.36</b>	<b>0.0202</b>
Left-Caudate	3705.7 $\pm$ 353.2	1.8	1.39	0.2223
Right-Caudate	3833.3 $\pm$ 396.3	0.8	0.41	0.6963
Left-Cerebellum-WM	14614.9 $\pm$ 1079.4	4.0	1.05	0.3391
Right-Cerebellum-WM	13845.8 $\pm$ 838.5	3.5	0.91	0.4052
Left-Cerebellum-Cortex	56577.2 $\pm$ 3483.4	0.0	0.01	0.9963
Right-Cerebellum-Cortex	56632.4 $\pm$ 3627.4	-0.0	-0.00	0.9989
Left-Pallidum	1931.5 $\pm$ 297.8	3.5	1.58	0.1746
Right-Pallidum	2046.3 $\pm$ 338.6	4.5	0.82	0.4484
Left-Putamen	5503.1 $\pm$ 340.4	-0.0	-0.02	0.9866
Right-Putamen	5553.7 $\pm$ 408.8	-0.6	-0.22	0.8349
Left-Accumbens-area	657.2 $\pm$ 39.5	-5.3	-0.70	0.5166
Right-Accumbens-area	665.8 $\pm$ 56.9	1.4	0.44	0.6800
Brain-Stem	22331.0 $\pm$ 1703.5	0.7	1.15	0.3026



Figures 4.2-4.5 show the absolute and relative values in percent for the left and right hippocampus, right amygdala and right thalamus, respectively. All of the volume change plots show an increase in volume, with the right hippocampus having the largest percent increase. This is consistent with the selected ROIs having a positive t-value and percent change in table 4.3.

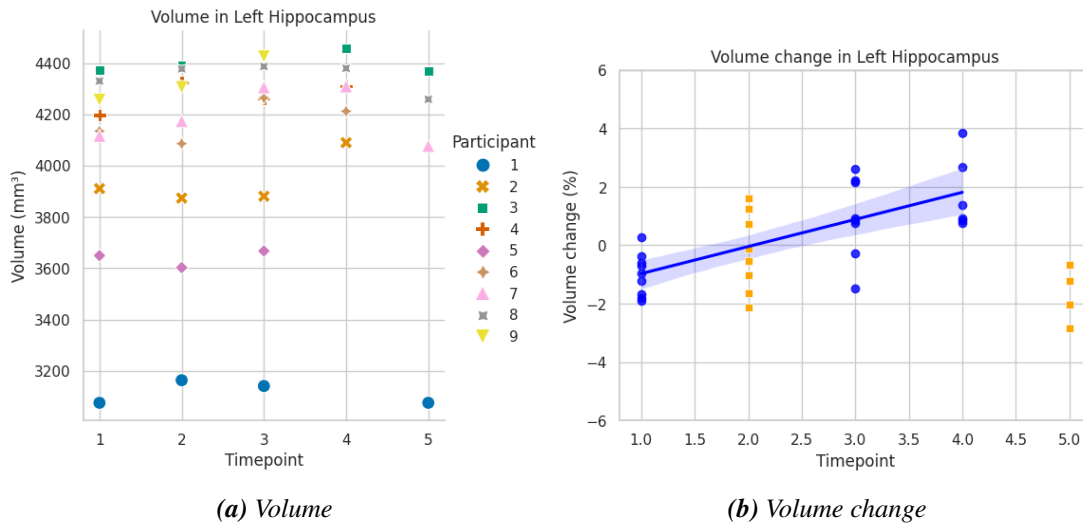


Figure 4.2: The volumetric measurements for left hippocampus in the ECT group.

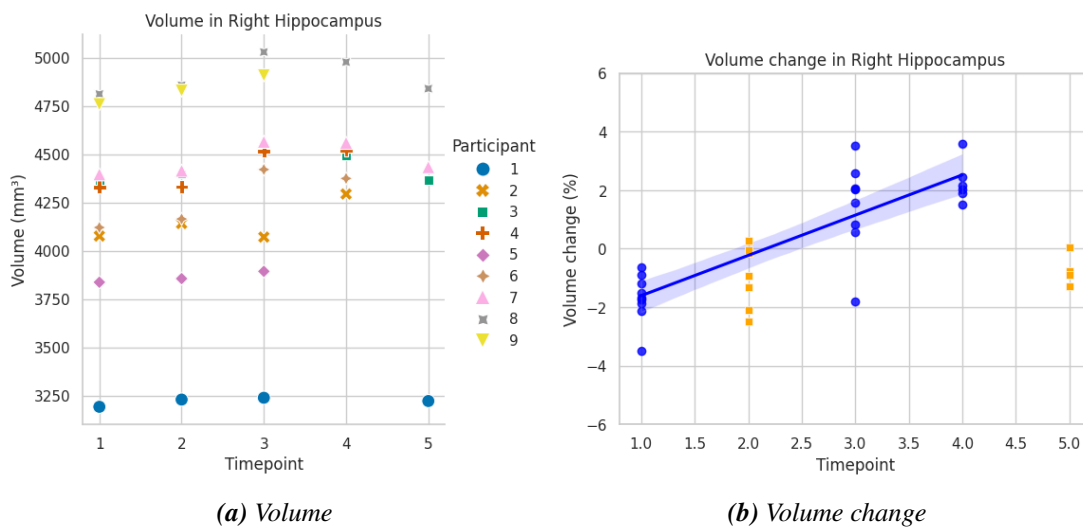


Figure 4.3: The volumetric measurements for right hippocampus in the ECT group.

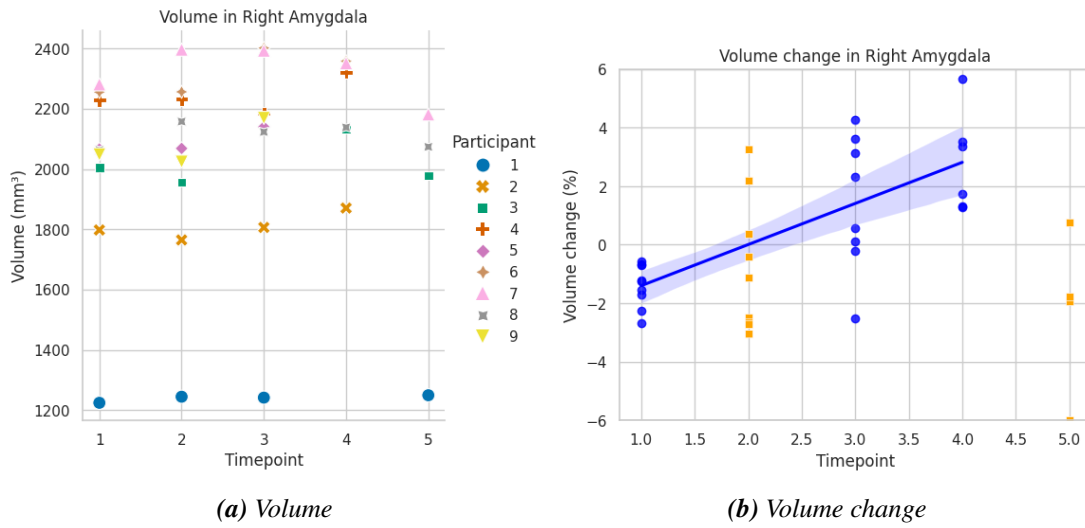


Figure 4.4: The volumetric measurements for right amygdala in the ECT group.

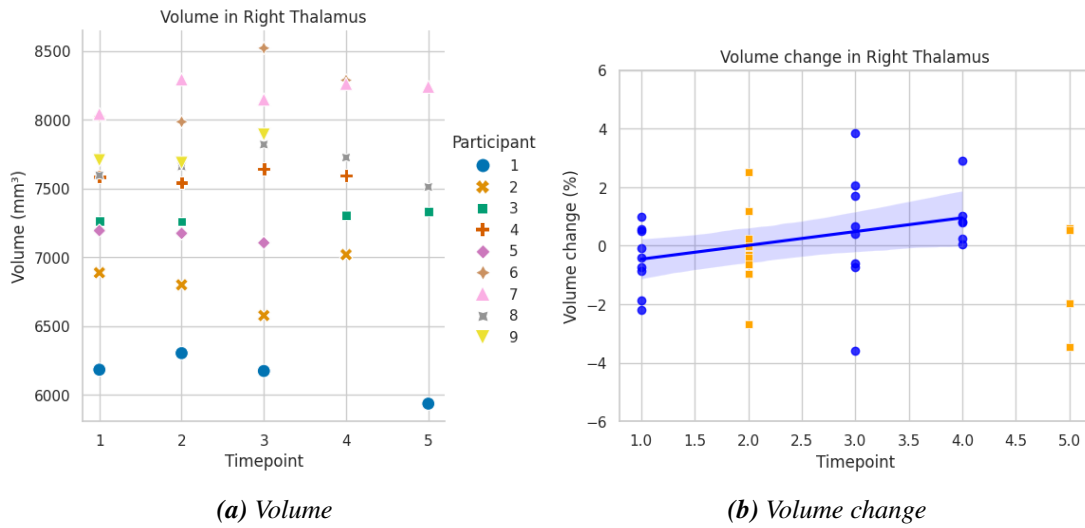


Figure 4.5: The volumetric measurements for right thalamus in the ECT group.

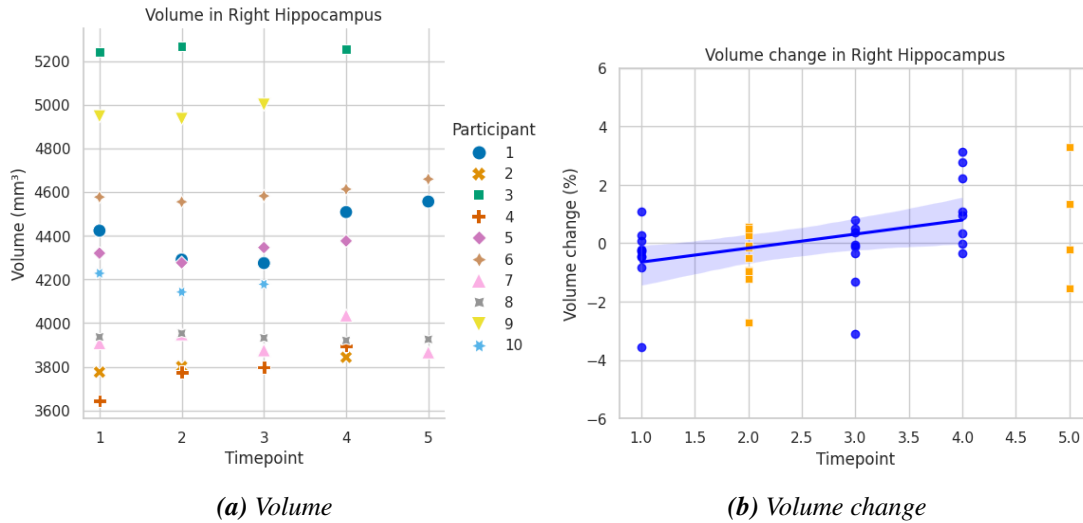
## TMS

Table 4.4 shows the mean values and standard deviations for scan 1 as well as the change in percent from scan 1 to scan 4, and the t-value and p-value for the volumes in the ROIs for the TMS group. The right hippocampus and right thalamus show a statistically significant increase with a p-value less than 0.05. None of the areas have a low enough p-value to pass the Bonferroni correction ( $p < 0.0026$ ).

**Table 4.4:** Mean value, standard deviation, percent change from scan 1 to scan 4 and p-value for the volumes in the ROIs for the TMS group. WM=White Mater, std=Standard Deviation

Areas	Scan 1 mean $\pm$ std ( $mm^3$ )	Change (%)	t-value	p-value
Left-Hippocampus	4161.2 $\pm$ 375.9	1.4	1.76	0.1210
<b>Right-Hippocampus</b>	<b>4228.9 <math>\pm</math> 491.8</b>	<b>1.8</b>	<b>2.63</b>	<b>0.0342</b>
Left-Amygdala	1758.8 $\pm$ 258.8	0.1	0.10	0.9239
Right-Amygdala	2058.7 $\pm$ 257.7	-0.8	-0.69	0.5119
Left-Thalamus	7681.4 $\pm$ 698.9	1.0	1.22	0.2615
<b>Right-Thalamus</b>	<b>7591.2 <math>\pm</math> 698.4</b>	<b>1.5</b>	<b>2.39</b>	<b>0.0482</b>
Left-Caudate	3818.7 $\pm$ 480.2	0.9	0.86	0.4176
Right-Caudate	3981.4 $\pm$ 440.0	0.1	0.12	0.9089
Left-Cerebellum-WM	14683.6 $\pm$ 2331.9	3.2	1.50	0.1776
Right-Cerebellum-WM	14635.5 $\pm$ 2545.3	4.4	2.20	0.0639
Left-Cerebellum-Cortex	57235.9 $\pm$ 3806.2	0.7	0.62	0.5536
Right-Cerebellum-Cortex	58284.6 $\pm$ 4071.4	1.1	0.56	0.5956
Left-Pallidum	1907.3 $\pm$ 207.8	-0.6	-0.96	0.3692
Right-Pallidum	1943.3 $\pm$ 224.9	0.4	0.36	0.7258
Left-Putamen	5165.5 $\pm$ 523.9	1.7	1.41	0.2011
Right-Putamen	5372.5 $\pm$ 491.3	1.4	1.32	0.2280
Left-Accumbens-area	591.8 $\pm$ 108.3	-1.3	-0.25	0.8123
Right-Accumbens-area	640.2 $\pm$ 67.4	0.4	0.28	0.7862
Brain-Stem	21551.2 $\pm$ 1630.5	0.9	1.97	0.0902

Figures 4.6 and 4.7 show the absolute and relative values in percent for right hippocampus and right thalamus, respectively. Both of the volume change plots show an increase in volume, which is consistent with the positive t-values and percent changes from table 4.4.



**Figure 4.6:** The volumetric measurements for Right Hippocampus in the TMS group.

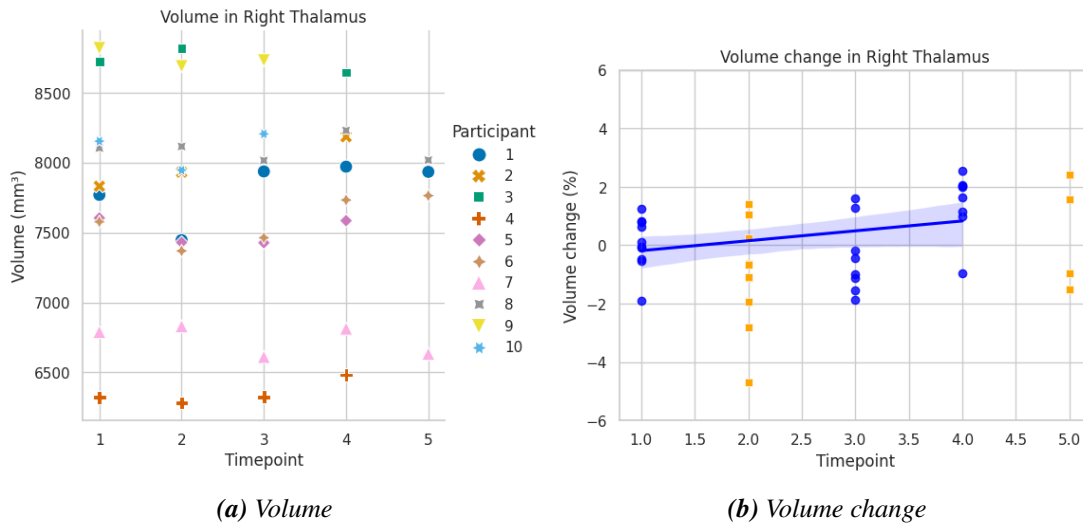


**Figure 4.7:** The volumetric measurements for Right Thalamus in the TMS group.

## 4.2 Perfusion change

The results in the previous section manifest volume change in specific brain structures but give little information on why the change occurs. In the current thesis, a primary goal is to investigate if there is an accompanying change in physiology, i.e. blood supply. Physiological changes do commonly precede structural changes. Because the same vascular tree is supplying the Hippocampus, Amygdala, and Thalamus and due to large variability, their analyses are grouped and will, from here on, be referred to as HAT.

### 4.2.1 Differences in baseline perfusion across groups

The following boxplots 4.8 show the initial difference in baseline perfusion in the HAT areas at scan 1. The boxplots show that the median value is slightly higher for the ECT group, but the difference from the control group is not significant (table 4.5).

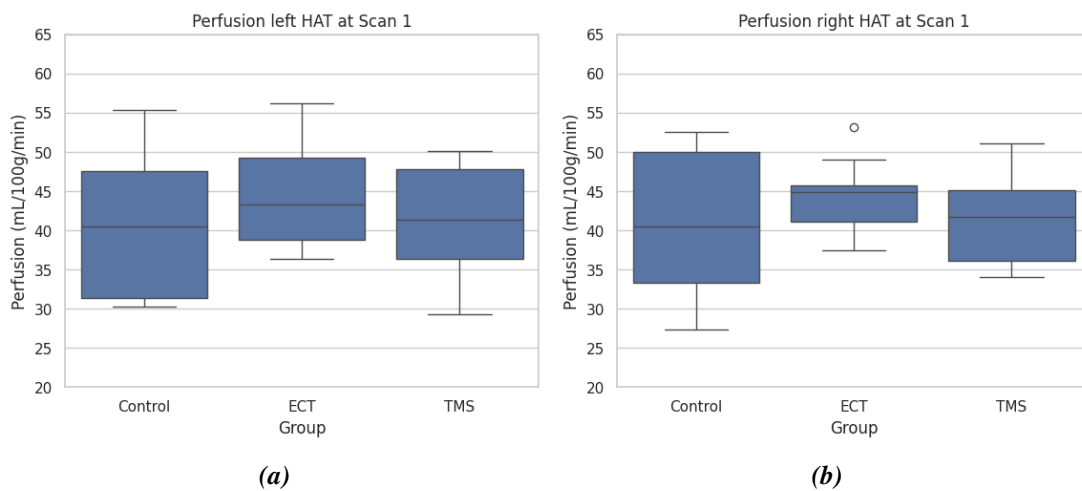


**Figure 4.8:** Perfusion in left (a) and right (b) Hippocampus, Amygdala, and Thalamus (HAT) at Scan 1.

Table 4.5 shows the resulting t-value and p-value after a two-sample t-test for independent samples (Welch's t-test) on perfusion at scan 1. The test was done to assess the difference between the control group and the ECT group or the TMS group, respectively. No statistical changes were found, but the ECT group show a slightly higher perfusion at baseline compared to the control group.

**Table 4.5:** *t*-value and *p*-value for the difference in perfusion between the control group and the ECT group or the TMS group, respectively, for the left (a) and right (a) hippocampus, amygdala and thalamus.

Group	t-value	p-value
ECT	0.67	0.5165
TMS	0.003	0.9979

(a) Left

Group	t-value	p-value
ECT	1.01	0.3308
TMS	0.27	0.7888

(b) Right

## 4.2.2 Longitudinal perfusion change

The tables 4.6, 4.7 and 4.8 show the mean perfusion values, as well as the laterality index for the control, ECT and TMS group over time, respectively. The laterality indexes have a low value, indicating no significant difference across the hemispheres in either group.

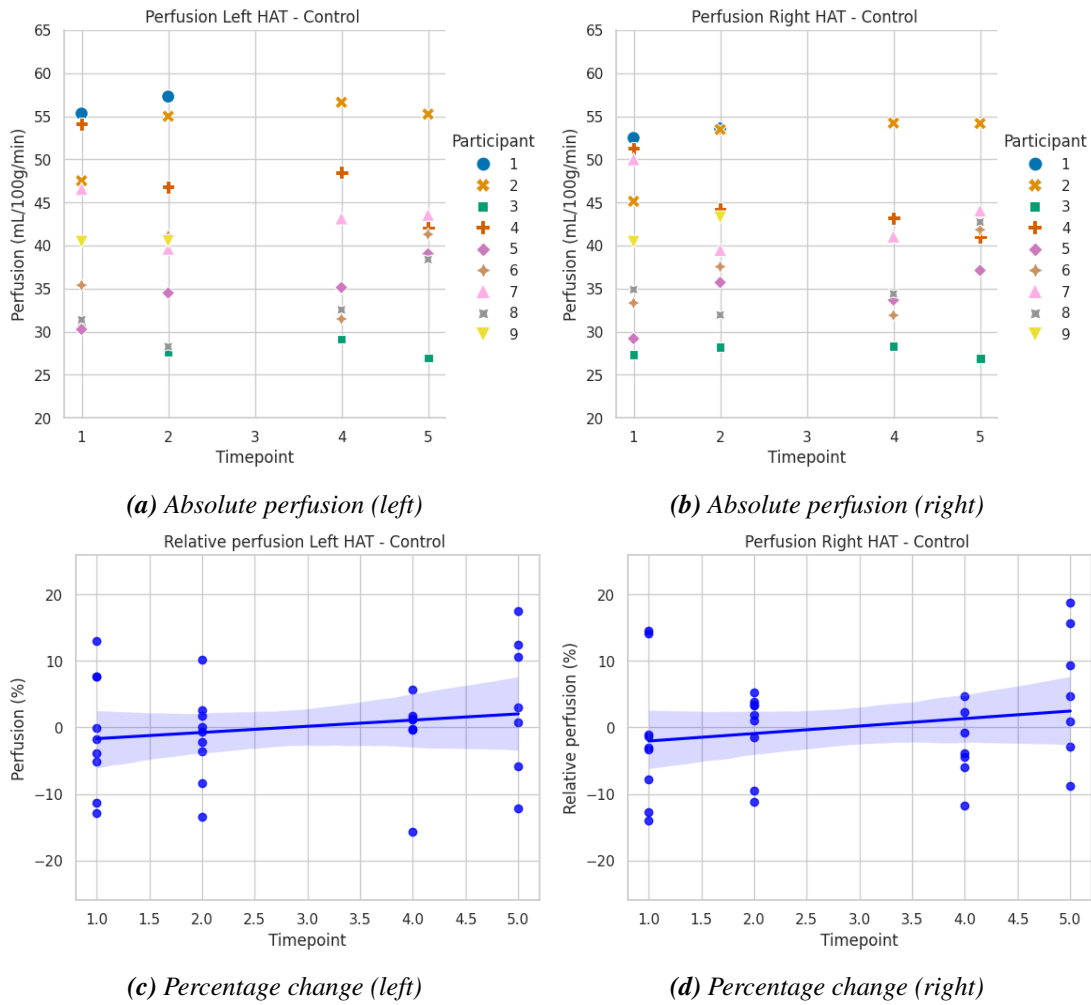
### Control

Table 4.6 shows the perfusion in left and right HAT for the control group, as well as the laterality index in percent. The *p*-value from table 4.9 shows there is no statistically significant change over time, which is to be expected from a control group. The values in table 4.6 assert the normal variation.

**Table 4.6:** Mean value of CBF in hippocampus, amygdala, and thalamus (HAT) and the laterality index in percent for the control group

	Scan 1	Scan 2	Scan 4	Scan 5
Laterality Index (%)	1.06	0.44	1.80	-0.21
CBF left HAT	41.3	41.2	39.5	40.9
CBF right HAT	40.5	40.8	38.1	41.1

Figure 4.9 shows the perfusion changes over time in left and right HAT for the control group. It shows no overall increase or decrease, which is consistent with the *t*- and *p*-values in table 4.9, and with table 4.6.



**Figure 4.9:** Plot of the perfusion in left and right Hippocampus, Amygdala and Thalamus (HAT) over time for the control group

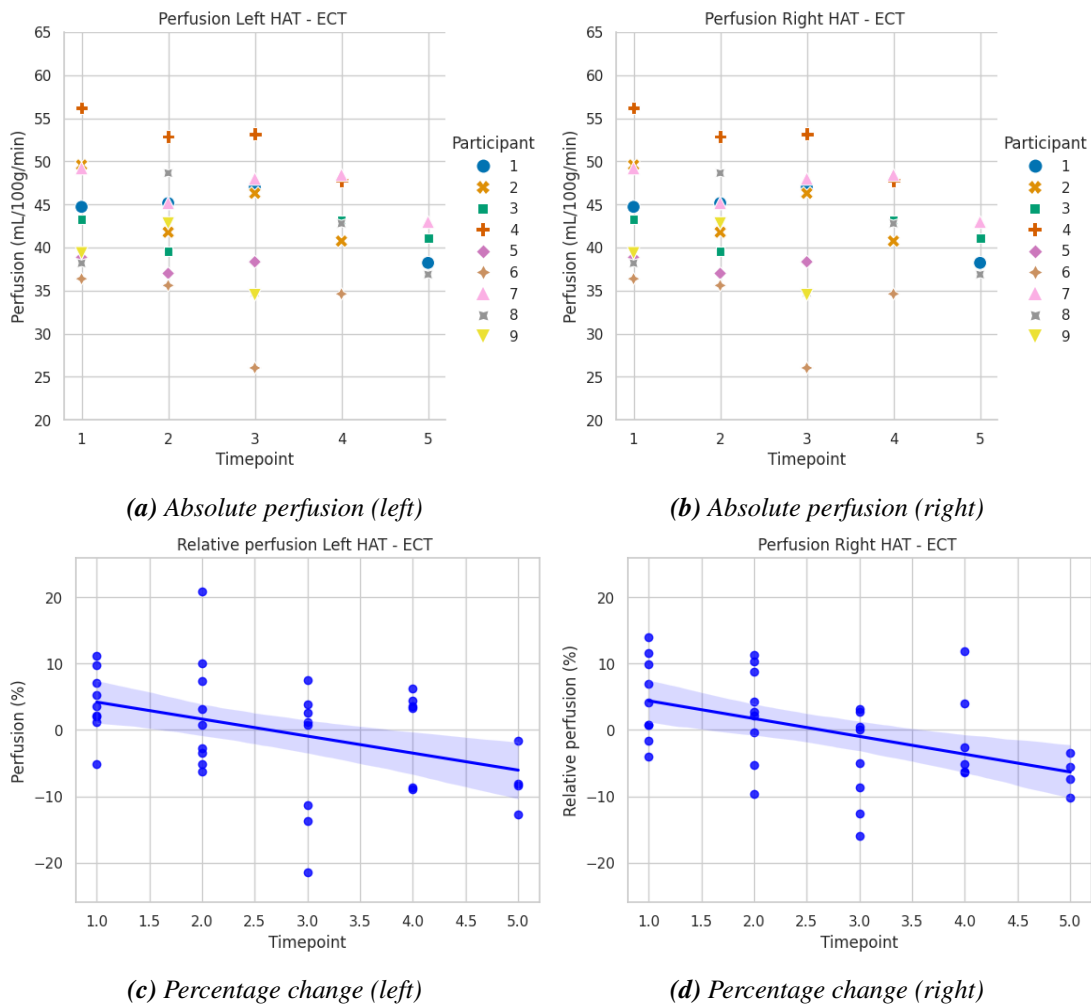
**ECT**

Table 4.7 shows the perfusion in the left and right HAT for the ECT group, as well as the laterality index. The perfusion values at scan 1 are slightly higher than their counterparts in the other two groups, but the p-values from table 4.5 (left:  $p = 0.5165$ , right:  $p = 0.3308$ ) don't indicate statistical significance. There is also a slight decrease in perfusion over time, but the p-values from table 4.9 don't indicate significance (left:  $p = 0.2843$ , right:  $p = 0.2886$ ).

**Table 4.7:** Mean value of CBF in HAT and the laterality index in percent for the ECT group

	Scan 1	Scan 2	Scan 3	Scan 4	Scan 5
Laterality Index (%)	-1.94	-0.08	0.68	0.70	0.39
CBF left	44.0	43.2	41.01	42.9	39.8
CBF right	44.1	43.3	40.5	42.3	39.5

Figure 4.10 shows the perfusion changes over time in left and right HAT for the ECT group. It shows a slight decrease for both sides, but the p-values from table 4.9 show change is not significant.



**Figure 4.10:** Plot of the perfusion in left and right Hippocampus, Amygdala and Thalamus (HAT) over time for the ECT group

## TMS

Table 4.8 shows the perfusion in left and right HAT for the TMS group, as well as the laterality index in percent. There seems to be an increase in the left HAT. No statistically significant changes were found between the TMS and control group (table 4.5), or over time (table 4.9).



**Table 4.8:** Mean value of CBF in HAT and the laterality index in percent for the TMS group

	Scan 1	Scan 2	Scan 3	Scan 4	Scan 5
Laterality Index (%)	-0.19	1.30	1.61	3.45	2.83
CBF left	41.3	42.4	41.0	42.6	43.3
CBF right	41.5	41.3	39.7	39.8	40.9

Figure 4.11 shows the perfusion changes over time in left and right HAT for the TMS group. The percentage plots show a "dip" in perfusion at scan 3.

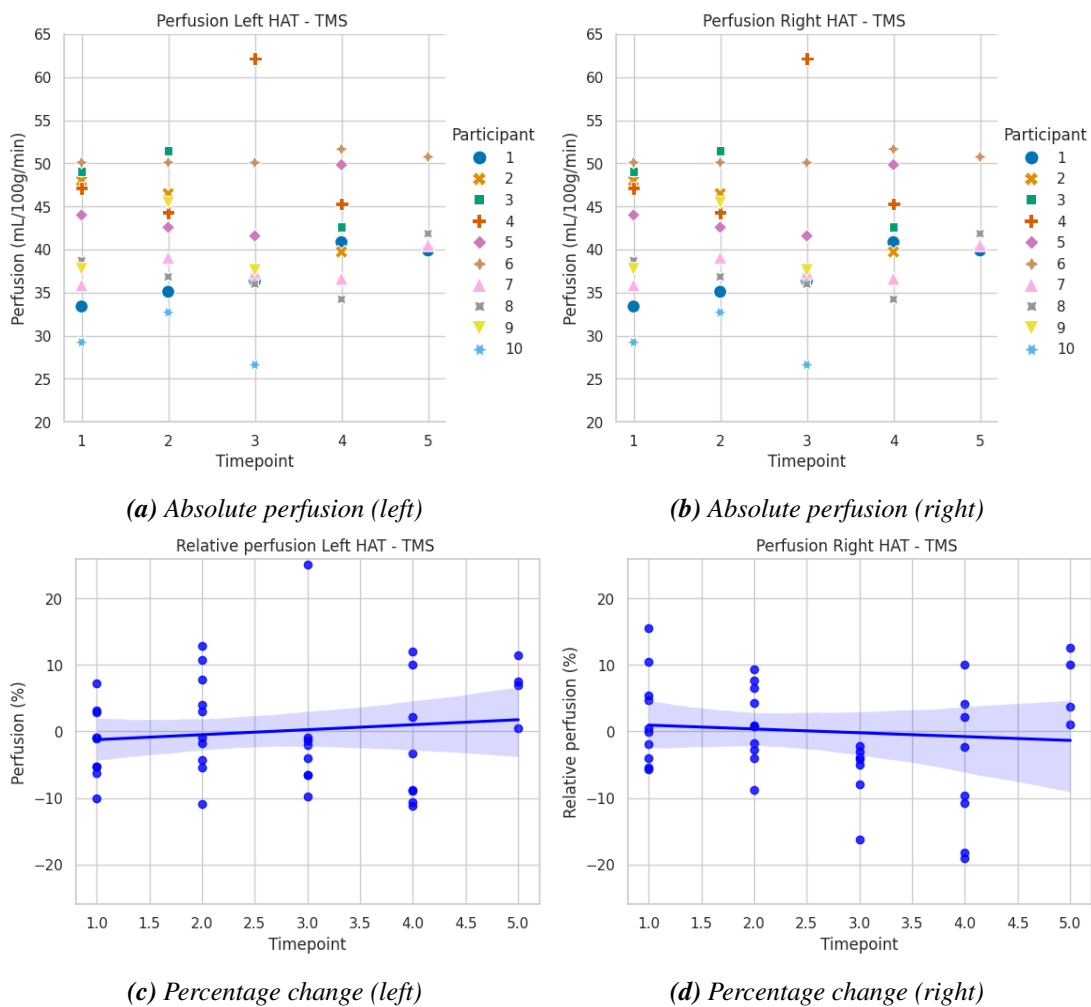


**Figure 4.11:** Plot of the perfusion in left and right Hippocampus, Amygdala and Thalamus (HAT) over time for the TMS group

**Longitudinal statistics** Table 4.9 shows the resulting t-values and the p-values after a paired t-test on the perfusion values. The test was performed on scan 1 and scan 4 for the HAT areas for both hemispheres. The table show no significant changes in perfusion for any of the groups.

**Table 4.9:** *t*-value and *p*-value for the change between scan 1 and scan 4 in the control, ECT, and TMS group, respectively.

Group	t-value	p-value
Control	0.03	0.9740
ECT	-1.20	0.2843
TMS	-0.34	0.7427

**(a)** *Left hippocampus, amygdala, and thalamus*

Group	t-value	p-value
Control	-0.26	0.8070
ECT	-1.19	0.2886
TMS	-1.23	0.2601

**(b)** *Right hippocampus, amygdala, and thalamus*

# Chapter 5

## Discussion and Conclusion

This project aimed to find a connection between brain perfusion and volume changes in areas of the brain. The connections were assessed by first finding the areas with a volumetric increase and then analyzing the perfusion in these areas.

This chapter discusses the results and any project limitations.

### 5.1 Volume change

The volumetric analysis studied the normal variation, variation across groups, and the effect of treatment. The analysis showed increased volume in the left and right hippocampus, right amygdala, and right thalamus for the ECT group and increased volume in the right hippocampus and right thalamus for the TMS group. Only the ECT group's right hippocampus and right amygdala pass the Bonferroni correction. The volumetric values from scan 4 were used to calculate the t-value and p-value for all the groups, as more participants had undergone scan 4 than scan 5, and scan 4 was the first after the end of the treatment. The volumetric increase in the ECT and TMS patients is expected to return to baseline by 7-8 months, meaning any volume increase would be lost by scan 5 [74][75].

#### 5.1.1 Normal variation

Table 4.1 presents the volumetric results for the control group. The table shows the mean value and standard deviation for all the participants in the group at scan 1 and the change in percent

from scan 1 to scan 4. As expected, the brain structures in the healthy participants show no significant change between the two scans, as all the areas have a p-value less than 0.05.

### 5.1.2 Variation across groups

The total intracranial volume was studied to assess variation across the groups before treatment. The results are presented in table 4.2 and visualized in figure 4.1. The analysis showed no difference in total intracranial volume beyond the standard deviations of each group. The lack of variation across groups is essential, showing that the data is comparable. If there were any differences in total intracranial volume, the volumetric data would have had to be accounted for in the analysis, as the volume of smaller structures depends on the total intracranial volume. Appendix A.1 shows the table of volumes divided by the total intracranial volume for scan 1 and scan 4 and the t-values and p-values for the control group. The table shows some change in the p-values as opposed to the values in table 4.1 from the volumetric analysis of the controls, but the difference from table 4.1 is small. Appendix A.2 and A.3 also show the tables for the ECT and TMS group, and no additional areas get a p-value less than 0.05 than in tables 4.3 and 4.4 from the volumetric analysis of the ECT and TMS group, respectively.

### 5.1.3 Effect of treatment

#### ECT

Table 4.3 presents the mean value and standard deviation for scan 1, the change in percent from scan 1 to scan 4, and the t-value and p-value from Welch's t-test for scan 1 and scan 4 for the ECT group. The table shows an increase in volume for the left ( $p < 0.01$ ) and right ( $p < 0.01$ ) hippocampus, right amygdala ( $p < 0.01$ ) and right thalamus ( $p < 0.05$ ). Previous studies [18] have also found a volume increase in these areas, meaning the findings are consistent with the literature. The right hippocampus and amygdala also pass the Bonferroni correction, indicating that they are not false positives due to multiple testing.

The figures 4.2-4.5 show the absolute and relative change in percent for the left and right hippocampus, right amygdala, and right thalamus, respectively. The plots showing the absolute values, figure (a) for figures 4.2-4.5, illustrate that the variations between participants are more extensive than those for individual participants. For instance, participant 1 (blue circle) has lower volumes than the other participants, but the change over time is relatively steady. The

large participant variability explains the need to compare the percentage volume change.

The plots presenting the percentage volume change, figure (b) for figures 4.2-4.5, show an increase in volume from scan 1 until scan 4 and a decrease by scan 5. Finding an increase followed by a decrease in such a small dataset with high statistical significance was expected yet interesting. Using scans 1, 3, and 4 (blue circles) as the basis for the regression line illustrates the increase over time.

The plots showing the percentage volume change, figure (b) for figures 4.2-4.4 for left and right hippocampus and right amygdala all show a distinct increase that corresponds with the change in percent in table 4.3. The percentage changes for left and right hippocampus and right amygdala are 2.8%, 4.3%, and 4.3%, respectively. Figure b for figure 4.5 shows the percentage volume change for the right thalamus. The figure shows how the volume increase is smaller than for the hippocampus and amygdala, which is consistent with a smaller change in percent from table 4.3 at 1.8%.

The left amygdala in table 4.3 shows a percent change of 3.7% with  $p = 0.0601$ . The p-value was not low enough to reject  $H_0$  for this area, but future dataset analyses should include a volumetric analysis of the left amygdala to investigate the increase.

## TMS

Table 4.4 presents the mean value and standard deviation for scan 1, the change in percent from scan 1 to scan 4, and the t-value and p-value from Welch's t-test for scan 1 and scan 4 for the TMS group. The right hippocampus and thalamus show a volumetric change with  $p < 0.05$ . The t-values ( $t=2.63$  and  $t=2.39$ , respectively) and changes in percent from scan 1 to scan 4 (1.8% and 1.5%, respectively) show increased volume for the hippocampus and thalamus. The increase is smaller than those found for the ECT participants in the same areas (4.3% and 1.8%, respectively). Lower volumetric increases for the TMS group than the ECT group were expected, as the field strength in the hippocampus and thalamus is lower for TMS than ECT. The p-values are also lower, with  $p = 0.0342$  and  $p = 0.0482$  for TMS and  $p = 0.0001$  and  $p = 0.0202$  for ECT. The p-values for the TMS group do not pass the Bonferroni correction, so these findings should be reviewed in later dataset analyses. The analysis found a volumetric change in the right hemisphere despite TMS being performed on the left hemisphere.

The plots showing the absolute volumetric values for the right hippocampus and right thalamus,

figure (a) for figures 4.6 and 4.7, show that there is a considerable variation between the participants. However, the variation for the individual participants is more stable, as was the case for the ECT group, explaining the need to compare the percentage volume change.

The plots showing the relative percent volume change, figure (b) for figures 4.6 and 4.7, show an increase in volume, but the change is not as prominent as the change for the ECT group in the same areas, which is consistent with the lower TMS field strength.

The field generated by the TMS treatment is generally not considered to reach subcortical areas such as the right hippocampus [13]. Yet, the analysis showed a volume increase in this area, as well as in the right thalamus. The p-values for these areas were  $p = 0.0342$  and  $p = 0.0482$ , respectively. These p-values barely pass the initial cutoff value at  $p = 0.05$  and do not pass the Bonferroni correction at  $p = 0.0026$ . When comparing the percent increase in these areas for the TMS (1.8% and 1.5% respectively) group to the control (-0.6% and 1.1%) group, both of the areas surpass the change in the control groups. However, the right hippocampus is far from reaching the change found in the area for the ECT group (4.5%), while the thalamus is closer (1.8%). This fits well with the fact that the TMS field is not as strong in these areas as the ECT field.

## 5.2 Perfusion change

### 5.2.1 Differences in baseline perfusion across groups

Figure 4.8 shows the perfusion in the left (4.8a) and right (4.8b) HAT at scan 1 for the different groups as two boxplots.

Figure 4.8a might indicate higher baseline perfusion in the ECT group than the control group for the left HAT, but the t-value ( $t = 0.67$ ) and p-value ( $p = 0.5165$ ) from table 4.5a indicates the change is not significant. The TMS group in figure 4.8a shows no difference in baseline perfusion from the control group for the left HAT, which is consistent with the t-value ( $t = 0.0027$ ) and p-value ( $p = 0.9979$ ) from table 4.5a.

Figure 4.8b might indicate a higher baseline perfusion in the ECT group than the control group for the right HAT, but the t-value ( $t = 1.01$ ) and p-value ( $p = 0.3308$ ) from table 4.5a indicates the change is not significant. However, the results from the right HAT look more promising

than the results from the left HAT and should be examined with a larger dataset in the future. The TMS group in figure 4.8b shows no difference in baseline perfusion from the control group for the right HAT, which is consistent with the t-value ( $t = 0.27$ ) and p-value ( $p = 0.7888$ ) from table 4.5b.

### 5.2.2 Longitudinal perfusion change

#### Control

Table 4.6 presents the mean value in the left and right HAT areas at all scans for the control group and the laterality index in percent. It shows how the perfusion varies over time and has no clear increase or decrease. This is consistent with the t-value ( $t = -0.26$ ) and p-value ( $p = 0.8070$ ) from table 4.9, as well as figure 4.9. The laterality index also shows no significant difference between the hemispheres. All the subplots in figure 4.9 show how the perfusion has a significantly larger variability for singular participants than the volumetric values. For instance, participant 2 (orange cross) in figure 4.9a has a perfusion value of around 47 at scan 1 and 55 at scan 2, or about 17% increase. None of the HAT areas showed a volumetric increase or decrease greater than 6%.

#### ECT

Table 4.7 presents the mean value in the left and right HAT areas at all scans for the ECT group and the laterality index. It shows a slight decrease in perfusion for both hemispheres, but the change is not significant, with a p-value from table 4.9 (left:  $p = 0.2843$ , right:  $p = 0.2886$ ). A larger dataset is required to pinpoint the significance, but it may indicate a trend worth exploring further. Figure 4.10 and the t-value in table 4.9 (left:  $p = -1.20$ , right:  $t = -1.19$ ) also show this decrease.

Figure 4.10 shows the absolute and relative perfusion values for left and right HAT for the ECT group. Figures 4.10a and 4.10b showing the absolute perfusion values show that several participants lack scans 4 and 5. Figures 4.10c and 4.10d show the relative change in perfusion. Figure 4.10d of the right HAT indicates an increase in scan 4 similar to the increase seen for the TMS group in figure 4.11, but the lack of data points at scan 5 makes it difficult to say. Scan 4 is the first scan after treatment, and the perfusion may revert to baseline. This analysis should be repeated after completing the dataset.

#### TMS

Table 4.8 presents the mean value in the left and right HAT areas at all scans for the TMS group and the laterality index in percent. The laterality index shows no significant difference between the two hemispheres.

Figure 4.11 shows the absolute and relative perfusion values for left and right HAT for the TMS group. Scan 3 shows a decrease in perfusion for both hemispheres, which is visible in all the subplots. The perfusion reverts to baseline at scan 4. The decrease followed by the increase is more prominent for the TMS group than the ECT group in figure 4.10, but this may be due to a more extensive set of data points at scan 4. This analysis should be repeated after completing the dataset.

## 5.3 Potential confounders

### 5.3.1 Dataset

The dataset has few participants, as it is not yet complete, and therefore lacks the statistical power to find small effect sizes. Trends and connections may be missed due to insubstantial data points to support them. There is also a risk of noise being interpreted as findings. This increases the risk of both Type I and Type II errors.

The small datasets make it difficult to differentiate between normal variations and the effects of groups and treatments. Larger groups would make it easier to pinpoint the distributions of the variations and how they overlap.

There are several different diagnostic groups in the dataset: bipolar, depressive episode, and recurrent depressive episodes. The diagnostic group may affect the volumetric increases or the perfusion changes. Patients with BD may receive ECT as a treatment for manic, depressive or mixed episodes, making it difficult to compare this group with patients with single or recurrent depressive episodes. The patients with recurrent depressive episodes may have lower left hippocampal volumes at baseline than patients with just one depressive episode due to days with depression and hippocampal volume being negatively correlated [49], which may affect the volume change.



### 5.3.2 Treatment

The treatments are not equal across individuals in the groups.

For the ECT group, the treatment is administered three times a week until remission or for a maximum of 18 treatments [56]. Some patients may get into remission after just, say, 10 treatments, while other patients may need all 18 treatments. As the total number of ECT treatments affects the volume change [15], knowing the individual number of treatments among the participants would lead to a more accurate analysis. This correction should be included in future analyses of the data.

The electrode placement may also vary in the ECT group. The treatment will initially be administered with RUL positioning, but if it is necessary for the patient, it will switch to BL placement.

The treatment was administered five times a week for the TMS group for 6 weeks [56]. The results are more comparable because the patients receive the same number of treatment sessions.

### 5.3.3 MRI Considerations

#### 5.3.4 Considerations of volume segmentation

The volumes assessed in this study are relatively small; for instance, the left hippocampus in the control group has a mean size of  $4344\text{mm}^3$ . Any errors in the segmentation will affect both the volume and the perfusion estimates. The mean and median values were used as bases throughout the project to minimize the effect of faulty segmentations.

#### 5.3.5 Considerations of perfusion estimation

Even though the total brain perfusion does not vary [30], the supply to the different regions varies depending on several factors. To account for the changes in perfusion throughout the day, all scans except scan 2 were performed at 08:00. Age is also an important factor in brain perfusion, and should be included in the analysis when the dataset is large enough.

The CBF images have relatively low resolution, at  $14\text{mm}^3$  voxel size, as opposed to the T1 images that have resolutions of 1mm. The low resolution increases the chance of including signals from other areas in the surrounding tissue. If these areas have lower or higher perfusion,

the results in the ROIs will be affected. To test for this effect, an erosion of the mask of the left hippocampus from a test set was used to calculate the perfusion in the area, and compared to the perfusion with the FreeSurfer mask. The perfusion in the eroded mask was increased by around  $1,5\text{mL}/100\text{g}/\text{min}$  for all timepoints in the set. The increased perfusion suggests that some areas surrounding the left hippocampus have lower CBF than the ROI, which might affect the study results. However, the difference falls within the normal variation seen in table 4.6, and the variation between participants far outweighs this difference. The eroded mask was discarded from the pipeline as it was around half the size of the original mask. If any sub-areas in the hippocampus receive more or less blood flow or react differently to the treatment, this would affect the results.

The processing of the labeled and control images was performed by the MRI scanner, and not using software like the FSL BASIL. As the calculated CBF value in a voxel depends on several approximated factors like blood relaxation time and blood-water partition coefficient, it would be useful to compare the CBF output from the scanner with an image processed using FSL BASIL. In this project, several attempts were made to process the raw data using FSL BASIL, but due to complications with the dataset, software and operating system the BASIL processing was dropped from the project.

## 5.4 Conclusion and future work

In future studies of perfusion and ECT, some extra analyses should be included. Simulations of the field strength in the different ROIs can improve the analysis. ROAST [76][77] and SimNIBS [78] are simulation packages used to simulate ECT and TMS, respectively. By simulating the fields, one can more accurately study the correlation between field strength and volume increase or perfusion changes. The differences between ECT and TMS are especially interesting here due to the large differences in field strength.

The analysis in this project should be run again on the data once the data collection is complete, to evaluate a larger dataset. As the goal is to collect data from around 50 participants per group, any missing correlations could be found, and the normal variations could be defined more clearly. Especially the trends from the perfusion analysis could be dismissed as noise or accepted as trends with a larger dataset, as well as the volume increases found in the TMS group.

Another interesting analysis would be separating the different diagnostic groups to pinpoint any differences. As there are three diagnostic groups included in the study, bipolar disorder, single depressive episode, and recurrent depressive episode, analyzing the difference in baseline perfusion and perfusion change between these groups could provide insight into the different diagnoses and how they affect the physiology.

This study aimed to investigate if there was a connection between changes in brain perfusion and volume changes in areas of the brain. In this thesis, I have successfully used FreeSurfer and FSL BASIL to analyze the MRI images from healthy controls, ECT and TMS participants in an ongoing clinical study. The analysis showed a volumetric increase in the left and right hippocampus, right amygdala, and right thalamus for the ECT group, but only the right hippocampus and amygdala passed a Bonferroni correction. The analysis also showed a volumetric increase in the right hippocampus and right thalamus for the TMS group, but none of the areas passed a Bonferroni correction. The perfusion analyses were combined for the Hippocampus, Amygdala, and Thalamus (HAT). There were no statistically significant changes between the groups at baseline perfusion, and none of the groups showed a statistically significant longitudinal increase or decrease. There were also no statistically significant differences across the hemispheres. Although not significant, there were trends showing a decrease in perfusion in the ECT group when investigating the rate of change in percent (%). Similarly, in the TMS group, trends showing a slight decrease followed by an increase were seen for the percent changes (%). There were also trends showing an increased baseline perfusion for the ECT group in both hemispheres. When more participants are included in the overall study, it can be verified whether these trends are true or random variations, as there were few participants at the time of the analysis and the perfusion data have larger variations than the volumetric data. The established pipeline can process image data from new participants as they join the study.

# Bibliography

- [1] *Depressive disorder (depression)*, 2023. [Online]. Available: <https://www.who.int/news-room/fact-sheets/detail/depression> (visited on 12/19/2023).
- [2] *Bipolar disorder*, Feb. 2024. [Online]. Available: <https://www.nimh.nih.gov/health/topics/bipolar-disorder> (visited on 05/21/2024).
- [3] D. Voineskos, Z. J. Daskalakis, and D. M. Blumberger, “Management of treatment-resistant depression: Challenges and strategies,” *Neuropsychiatric Disease and Treatment*, vol. 16, pp. 221–234, 2020, ISSN: 11782021. DOI: 10.2147/NDT.S198774.
- [4] I. Dalhuisen, E. Ackermans, L. Martens, *et al.*, “Longitudinal effects of rTMS on neuroplasticity in chronic treatment-resistant depression,” *European Archives of Psychiatry and Clinical Neuroscience*, vol. 271, pp. 39–47, 1 Feb. 2021, ISSN: 14338491. DOI: 10.1007/s00406-020-01135-w.
- [5] M. Argyelan, L. Oltedal, Z. D. Deng, *et al.*, “Electric field causes volumetric changes in the human brain,” *eLife*, vol. 8, Oct. 2019, ISSN: 2050084X. DOI: 10.7554/eLife.49115.
- [6] J. Yang, H. Guo, A. Cai, *et al.*, “Aberrant hippocampal development in early-onset mental disorders and promising interventions: Evidence from a translational study,” *Neuroscience Bulletin*, 2023, ISSN: 19958218. DOI: 10.1007/s12264-023-01162-2.
- [7] A. M. Leaver, M. Vasavada, A. Kubicki, *et al.*, “Hippocampal subregions and networks linked with antidepressant response to electroconvulsive therapy,” *Molecular Psychiatry*, vol. 26, pp. 4288–4299, 8 Aug. 2021, ISSN: 14765578. DOI: 10.1038/s41380-020-0666-z.
- [8] *Freesurfer*. [Online]. Available: <https://surfer.nmr.mgh.harvard.edu/> (visited on 02/26/2024).

- [9] *Basil*. [Online]. Available: <https://fsl.fmrib.ox.ac.uk/fsl/fslwiki/BASIL> (visited on 02/26/2024).
- [10] *Major depressive disorder—level 4 cause*, Oct. 2020. [Online]. Available: <https://www.thelancet.com/pb-assets/Lancet/gbd/summaries/diseases/major-depressive-disorder.pdf> (visited on 01/10/2024).
- [11] G. Perugi, P. Medda, C. Toni, M. G. Mariani, C. Socci, and M. Mauri, “The role of electroconvulsive therapy (ect) in bipolar disorder: Effectiveness in 522 patients with bipolar depression, mixed-state, mania and catatonic features,” *Current Neuropharmacology*, vol. 15, pp. 359–371, 2017. DOI: 10.2174/1570159X14666161017233.
- [12] W. McDonald and L. Fochtmann, *What is electroconvulsive therapy (ect)?* American Psychiatric Association, 2023. [Online]. Available: <https://www.who.int/news-room/fact-sheets/detail/depression> (visited on 12/19/2023).
- [13] W. Klomjai, R. Katz, and A. Lackmy-Vallée, *Basic principles of transcranial magnetic stimulation (tms) and repetitive tms (rtms)*, Sep. 2015. DOI: 10.1016/j.rehab.2015.05.005.
- [14] V. Walsh and A. Cowey, *Transcranial magnetic stimulation and cognitive neuroscience*, 2000. [Online]. Available: <https://www.nature.com/articles/35036239>.
- [15] L. Oltegal, K. L. Narr, C. Abbott, *et al.*, “Volume of the human hippocampus and clinical response following electroconvulsive therapy,” *Biological Psychiatry*, vol. 84, pp. 574–581, 8 Oct. 2018, ISSN: 18732402. DOI: 10.1016/j.biopsych.2018.05.017.
- [16] L. Oltegal, U. Kessler, L. Ersland, *et al.*, “Effects of ect in treatment of depression: Study protocol for a prospective neuroradiological study of acute and longitudinal effects on brain structure and function,” *BMC Psychiatry*, vol. 15, 1 May 2015, ISSN: 1471244X. DOI: 10.1186/s12888-015-0477-y.
- [17] O. T. Ousdal, G. E. Brancati, U. Kessler, *et al.*, “The neurobiological effects of electroconvulsive therapy studied through magnetic resonance: What have we learned, and where do we go?” *Biological Psychiatry*, vol. 91, pp. 540–549, 6 Mar. 2022, ISSN: 0006-3223. DOI: 10.1016/J.BIOPSYCH.2021.05.023.
- [18] O. T. Ousdal, M. Argyelan, K. L. Narr, *et al.*, “Brain changes induced by electroconvulsive therapy are broadly distributed,” *Biological Psychiatry*, vol. 87, pp. 451–461, 5 Mar. 2020, ISSN: 18732402. DOI: 10.1016/j.biopsych.2019.07.010.

- [19] A. M. Leaver, M. Vasavada, S. H. Joshi, *et al.*, “Mechanisms of antidepressant response to electroconvulsive therapy studied with perfusion magnetic resonance imaging,” *Biological Psychiatry*, vol. 85, pp. 466–476, 6 Mar. 2019, ISSN: 18732402. DOI: 10.1016/j.biopsych.2018.09.021.
- [20] J. C. M. Pottkämper, J. P. A. J. Verdijk, E. Aalbrecht, *et al.*, “Changes in postictal cerebral perfusion are related to the duration of electroconvulsive therapy-induced seizures,” *Epilepsia*, Nov. 2023, ISSN: 0013-9580. DOI: 10.1111/epi.17831.
- [21] R. W. Brown, Y. C. N. Cheng, E. M. Haacke, M. R. Thompson, and R. Venkatesan, *Magnetic Resonance Imaging : Physical Principles and Sequence Design*. John Wiley & Sons, Incorporated, 2014, ISBN: 978-0-471-72085-0.
- [22] D. J. Griffiths, *Introduction to Electrodynamics*, 4th ed. Pearson Education Inc., 2013, ISBN: 978-0-321-85656-2.
- [23] H. D. Young and R. A. Freedman, *University Physics with Modern Physics, Global Edition*, 15th ed. Pearson Education Limited, 2020, ISBN: 978-1-292-31473-0.
- [24] T. Wagner, F. Fregni, S. Fecteau, A. Grodzinsky, M. Zahn, and A. Pascual-Leone, “Transcranial direct current stimulation: A computer-based human model study,” *NeuroImage*, vol. 35, pp. 1113–1124, 3 Apr. 2007, ISSN: 10538119. DOI: 10.1016/j.neuroimage.2007.01.027.
- [25] A. Datta, V. Bansal, J. Diaz, J. Patel, D. Reato, and M. Bikson, “Gyri-precise head model of transcranial direct current stimulation: Improved spatial focality using a ring electrode versus conventional rectangular pad,” *Brain Stimulation*, vol. 2, 4 2009, ISSN: 1935861X. DOI: 10.1016/j.brs.2009.03.005.
- [26] D. W. McRobbie, E. A. Moore, M. J. Graves, and M. R. Prince, *MRI from Picture to Proton*. Cambridge University Press, Apr. 2017, ISBN: 9781107706958. DOI: 10.1017/9781107706958. [Online]. Available: <https://www.cambridge.org/core/product/identifier/9781107706958/type/book>.
- [27] C. Westbrook, C. K. Roth, and J. Talbot, *MRI in Practice*, 4th ed. Wiley-Blackwell, 2011, ISBN: 978-1-4443-3743-3.
- [28] A. Alsaedi, D. Thomas, S. Bisdas, and X. Golay, “Overview and critical appraisal of arterial spin labelling technique in brain perfusion imaging,” *Contrast Media & Molecular Imaging*, vol. 2018, pp. 1–15, 2018, ISSN: 1555-4309. DOI: 10.1155/2018/5360375.

- [29] P. Clement, J. Petr, M. B. J. Dijsselhof, *et al.*, “A beginner’s guide to arterial spin labeling (asl) image processing,” *Frontiers in Radiology*, vol. 2, Jun. 2022. DOI: 10.3389/fradi.2022.929533.
- [30] O. Sand, Ø. V. Sjaastad, and E. Haug, *Menneskets fysiologi*, 2nd ed. Gyldendal, 2018, ISBN: 978-82-05-42341-1.
- [31] D. C. Alsop, J. A. Detre, X. Golay, *et al.*, *Recommended implementation of arterial spin labeled perfusion mri for clinical applications: A consensus of the ismrm perfusion study group and the european consortium for asl in dementia*, Oct. 2015. DOI: 10.1002/mrm.25197.
- [32] T. Elvsåshagen, H. J. Mutsaerts, N. Zak, *et al.*, “Cerebral blood flow changes after a day of wake, sleep, and sleep deprivation,” *NeuroImage*, vol. 186, pp. 497–509, Feb. 2019, ISSN: 10959572. DOI: 10.1016/j.neuroimage.2018.11.032.
- [33] P. Clement, H. J. Mutsaerts, L. Václavů, *et al.*, *Variability of physiological brain perfusion in healthy subjects – a systematic review of modifiers. considerations for multi-center asl studies*, Sep. 2018. DOI: 10.1177/0271678X17702156.
- [34] C. M. Swartz, *Guide to electroconvulsive therapy*, 2015.
- [35] C. H. Kellner, K. G. Tobias, and J. Wiegand, *Electrode placement in electroconvulsive therapy (ect): A review of the literature*, Sep. 2010. DOI: 10.1097/YCT.0b013e3181e48154.
- [36] A. Singh and S. K. Kar, “How electroconvulsive therapy works?: Understanding the neurobiological mechanisms,” *Clinical Psychopharmacology and Neuroscience*, vol. 15, pp. 210–221, 3 Aug. 2017, ISSN: 1738-1088. DOI: 10.9758/cpn.2017.15.3.210.
- [37] *Icd-10 og icd-11*. [Online]. Available: <https://www.ehelse.no/kodeverk-og-terminologi/ICD-10-og-ICD-11> (visited on 05/14/2024).
- [38] *Icd-10 - den internasjonale statistiske klassifikasjonen av sykdommer og beslektede helseproblemer*. [Online]. Available: <https://finnkode.ehelse.no/#icd10/0/0/0/-1> (visited on 05/13/2024).
- [39] U. M. (UiO), *Madrs*, Oct. 2019. [Online]. Available: <https://sml.snl.no/MADRS> (visited on 05/14/2024).
- [40] *Montgomery-åsberg depression rating scale*, Apr. 2024. [Online]. Available: [https://en.wikipedia.org/wiki/Montgomery%E2%80%93Asberg\\_Depression\\_Rating\\_Scale](https://en.wikipedia.org/wiki/Montgomery%E2%80%93Asberg_Depression_Rating_Scale) (visited on 05/14/2024).

- [41] G. L. Faedda, I. Becker, A. Baroni, L. Tondo, E. Aspland, and A. Koukopoulos, *The origins of electroconvulsive therapy: Prof. bini's first report on ect*, Jan. 2010. DOI: 10.1016/j.jad.2009.01.023.
- [42] G. Gazdag and G. S. Ungvari, "Electroconvulsive therapy: 80 years old and still going strong," *World Journal of Psychiatry*, vol. 9, pp. 1–6, 1 Jan. 2019, ISSN: 2220-3206. DOI: 10.5498/wjp.v9.i1.1.
- [43] T. G. Bolwig, *How does electroconvulsive therapy work? theories on its mechanism*, 2011. DOI: 10.1177/070674371105600104.
- [44] R. J. Porter, B. T. Baune, G. Morris, *et al.*, "Cognitive side-effects of electroconvulsive therapy: What are they, how to monitor them and what to tell patients," *BJPsych Open*, vol. 6, 3 May 2020. DOI: 10.1192/bjo.2020.17.
- [45] M. Semkowska and D. M. McLoughlin, "Objective cognitive performance associated with electroconvulsive therapy for depression: A systematic review and meta-analysis," *Biological Psychiatry*, vol. 68, pp. 568–577, 6 Sep. 2010, ISSN: 00063223. DOI: 10.1016/j.biopsych.2010.06.009.
- [46] J. K. S. Jansen and P. Holck, *Hippocampus*, 2023. [Online]. Available: <https://sml.sn1.no/hippocampus> (visited on 12/16/2023).
- [47] L. Schmaal, D. J. Veltman, T. G. V. Erp, *et al.*, "Subcortical brain alterations in major depressive disorder: Findings from the enigma major depressive disorder working group," *Molecular Psychiatry*, vol. 21, pp. 806–812, 6 Jun. 2016, ISSN: 14765578. DOI: 10.1038/mp.2015.69.
- [48] S. H. Joshi, R. T. Espinoza, T. Pirnia, *et al.*, "Structural plasticity of the hippocampus and amygdala induced by electroconvulsive therapy in major depression," *Biological Psychiatry*, vol. 79, pp. 282–292, 4 Feb. 2016, ISSN: 18732402. DOI: 10.1016/j.biopsych.2015.02.029.
- [49] Y. I. Sheline, P. W. Wang, M. H. Gado, J. G. Csernansky, and M. W. Vannier, "Hippocampal atrophy in recurrent major depression," *Proceedings of the National Academy of Sciences (PNAS), of the United States of America, Medical Sciences*, vol. 93, pp. 3908–3913, 1996. DOI: 10.1073/pnas.93.9.3908.
- [50] M. Argyelan, T. Lencz, S. Kang, *et al.*, "Ect-induced cognitive side effects are associated with hippocampal enlargement," *Translational Psychiatry*, vol. 11, 1 Dec. 2021, ISSN: 21583188. DOI: 10.1038/s41398-021-01641-y.



- [51] I. Mossige, “Volume increase of the hippocampus after electroconvulsive therapy,” M.S. thesis, University of Bergen, 2021.
- [52] L. G. Chepenik, F. Wang, L. Spencer, *et al.*, “Structure-function associations in hippocampus in bipolar disorder,” *Biological Psychology*, vol. 90, pp. 18–22, 1 Apr. 2012, ISSN: 03010511. DOI: 10.1016/j.biopsycho.2012.01.008.
- [53] H. Takano, N. Motohashi, T. Uema, *et al.*, “Changes in regional cerebral blood flow during acute electroconvulsive therapy in patients with depression: Positron emission tomographic study,” *British Journal of Psychiatry*, vol. 190, no. 1, pp. 63–68, 2007. DOI: 10.1192/bjp.bp.106.023036.
- [54] T. Suwa, C. Namiki, S. Takaya, *et al.*, “Corticolimbic balance shift of regional glucose metabolism in depressed patients treated with ect,” *Journal of Affective Disorders*, vol. 136, pp. 1039–1046, 3 Feb. 2012, ISSN: 01650327. DOI: 10.1016/j.jad.2011.11.040.
- [55] M. S. Nobler, M. A. Oquendo, L. S. Kegeles, *et al.*, *Decreased regional brain metabolism after ect*, 2001. DOI: 10.1176/appi.ajp.158.2.305.
- [56] L. M. Frid, U. Kessler, O. T. Ousdal, *et al.*, “Neurobiological mechanisms of ect and tms treatment in depression: Study protocol of a multimodal magnetic resonance investigation,” *BMC Psychiatry*, vol. 23, p. 791, 1 Oct. 2023, ISSN: 1471-244X. DOI: 10.1186/s12888-023-05239-0. [Online]. Available: <https://bmcp psychiatry.biomedcentral.com/articles/10.1186/s12888-023-05239-0>.
- [57] M. Fogarty, *Recon-all*, Dec. 2017. [Online]. Available: <https://surfer.nmr.mgh.harvard.edu/fswiki/recon-all> (visited on 02/26/2024).
- [58] D. Cordero, *Longitudinal processing*, May 2021. [Online]. Available: <https://surfer.nmr.mgh.harvard.edu/fswiki/LongitudinalProcessing> (visited on 02/27/2024).
- [59] M. Reuter, N. J. Schmansky, H. D. Rosas, and B. Fischl, “Within-subject template estimation for unbiased longitudinal image analysis,” *NeuroImage*, vol. 61, no. 4, pp. 1402–1418, 2012. DOI: 10.1016/j.neuroimage.2012.02.084. [Online]. Available: <http://dx.doi.org/10.1016/j.neuroimage.2012.02.084>.
- [60] M. Fogarty, *Longitudinal statistics*, Jul. 2018. [Online]. Available: <https://surfer.nmr.mgh.harvard.edu/fswiki/LongitudinalStatistics> (visited on 03/04/2024).
- [61] M. Ebling, *Asegstats2table*, Dec. 2012. [Online]. Available: <https://surfer.nmr.mgh.harvard.edu/fswiki/asegstats2table> (visited on 03/04/2024).

- [62] M. L. Waskom, “Seaborn: Statistical data visualization,” *Journal of Open Source Software*, vol. 6, no. 60, p. 3021, 2021. DOI: 10.21105/joss.03021. [Online]. Available: <https://doi.org/10.21105/joss.03021>.
- [63] J. D. Hunter, “Matplotlib: A 2d graphics environment,” *Computing in Science & Engineering*, vol. 9, no. 3, pp. 90–95, 2007. DOI: 10.1109/MCSE.2007.55.
- [64] P. Virtanen, R. Gommers, T. E. Oliphant, *et al.*, “SciPy 1.0: Fundamental Algorithms for Scientific Computing in Python,” *Nature Methods*, vol. 17, pp. 261–272, 2020. DOI: 10.1038/s41592-019-0686-2.
- [65] T. pandas development team, *Pandas-dev/pandas: Pandas*, version latest, Feb. 2020. DOI: 10.5281/zenodo.3509134. [Online]. Available: <https://doi.org/10.5281/zenodo.3509134>.
- [66] C. R. Harris, K. J. Millman, S. J. van der Walt, *et al.*, “Array programming with NumPy,” *Nature*, vol. 585, no. 7825, pp. 357–362, Sep. 2020. DOI: 10.1038/s41586-020-2649-2. [Online]. Available: <https://doi.org/10.1038/s41586-020-2649-2>.
- [67] J. L. Devore, K. N. Berk, and M. A. Carlton, *Modern Mathematical Statistics with Applications*, 3rd ed., G. Allen, R. D. Veaux, and R. Nugent, Eds. Springer, 2021, ISBN: 978-3-030-55155-1.
- [68] *Students t-test*, Feb. 2024. [Online]. Available: [https://en.wikipedia.org/wiki/Student%27s\\_t-test](https://en.wikipedia.org/wiki/Student%27s_t-test) (visited on 04/22/2024).
- [69] *Scipy.stats.ttest\_rel*. [Online]. Available: [https://docs.scipy.org/doc/scipy/reference/generated/scipy.stats.ttest\\_rel.html#scipy.stats.ttest\\_rel](https://docs.scipy.org/doc/scipy/reference/generated/scipy.stats.ttest_rel.html#scipy.stats.ttest_rel) (visited on 04/22/2024).
- [70] *Welch’s t-test*. [Online]. Available: [https://en.wikipedia.org/wiki/Welch%27s\\_t-test](https://en.wikipedia.org/wiki/Welch%27s_t-test) (visited on 05/15/2024).
- [71] *Scipy.stats.ttest\_ind*. [Online]. Available: [https://docs.scipy.org/doc/scipy/reference/generated/scipy.stats.ttest\\_ind.html](https://docs.scipy.org/doc/scipy/reference/generated/scipy.stats.ttest_ind.html) (visited on 05/14/2024).
- [72] *Bonferroni correction*, Online, Mar. 2024. [Online]. Available: [https://en.wikipedia.org/wiki/Bonferroni\\_correction](https://en.wikipedia.org/wiki/Bonferroni_correction) (visited on 04/22/2024).
- [73] *Multiple comparisons problem*, Online, Mar. 2024. [Online]. Available: [https://en.wikipedia.org/wiki/Multiple\\_comparisons\\_problem](https://en.wikipedia.org/wiki/Multiple_comparisons_problem) (visited on 04/22/2024).
- [74] P. Nordanskog, M. R. Larsson, E. M. Larsson, and A. Johanson, “Hippocampal volume in relation to clinical and cognitive outcome after electroconvulsive therapy in depression,”

- Acta Psychiatrica Scandinavica*, vol. 129, pp. 303–311, 4 2014, ISSN: 16000447. DOI: 10.1111/acps.12150.
- [75] F. Bouckaert, A. Dols, L. Emsell, *et al.*, “Relationship between hippocampal volume, serum bdnf, and depression severity following electroconvulsive therapy in late-life depression,” *Neuropsychopharmacology*, vol. 41, pp. 2741–2748, 11 Oct. 2016, ISSN: 1740634X. DOI: 10.1038/npp.2016.86.
- [76] Y. Huang, A. Datta, M. Bikson, and L. C. Parra, “Roast: An open-source, fully-automated, realistic volumetric-approach-based simulator for tes.,” *Annual International Conference of the IEEE Engineering in Medicine and Biology Society. IEEE Engineering in Medicine and Biology Society. Annual International Conference*, vol. 2018, pp. 3072–3075, Jul. 2018, ISSN: 2694-0604. DOI: 10.1109/EMBC.2018.8513086.
- [77] “Realistic volumetric-approach to simulate transcranial electric stimulation - roast - a fully automated open-source pipeline,” *Journal of Neural Engineering*, vol. 16, 5 Jul. 2019, ISSN: 17412552. DOI: 10.1088/1741-2552/ab208d.
- [78] A. Thielscher, A. Antunes, and G. B. Saturnino, “Field modeling for transcranial magnetic stimulation: A useful tool to understand the physiological effects of tms?” In *2015 37th Annual International Conference of the IEEE Engineering in Medicine and Biology Society (EMBC)*, 2015, pp. 222–225. DOI: 10.1109/EMBC.2015.7318340.

# Appendix A

## Additional tables

### A.1 Relative volumetric values for the control group

The volumetric values in the ROIs divided by the estimated total intracranial volume to account for different head sizes.

*Table A.1: Relative mean value, standard deviation and p-value for the volumes in the ROIs for the control group. WM = White Matter, std = Standard Deviation*

Areas	Scan 1 mean	Scan 1 std	Scan 4 mean	Scan 4 std	t-value	p-value
Left-Hippocampus	0.002701	0.000274	0.002711	0.000279	1.105	0.311322
Right-Hippocampus	0.002739	0.000272	0.002722	0.000274	-1.342	0.228095
Left-Amygdala	0.001093	0.000131	0.001072	0.000119	-1.795	0.122836
Right-Amygdala	0.001262	0.000109	0.001255	0.000079	-0.505	0.631486
Left-Thalamus	0.004837	0.000628	0.004876	0.000635	1.437	0.200736
Right-Thalamus	0.004697	0.000555	0.004755	0.000578	1.925	0.102509
Left-Caudate	0.002535	0.000309	0.002529	0.000315	-0.524	0.618910
Right-Caudate	0.002633	0.000316	0.002626	0.000330	-0.570	0.589417
Left-Cerebellum-WM	0.009403	0.001580	0.009456	0.001465	0.440	0.675417
Right-Cerebellum-WM	0.008850	0.001330	0.008811	0.001332	-0.907	0.399497
Left-Cerebellum-Cortex	0.036296	0.003232	0.036109	0.003070	-1.378	0.217480
Right-Cerebellum-Cortex	0.037052	0.003520	0.036757	0.003303	-2.403	0.053090
Left-Pallidum	0.001314	0.000092	0.001322	0.000101	0.812	0.447867
Right-Pallidum	0.001334	0.000097	0.001342	0.000107	0.816	0.445678
Left-Putamen	0.003468	0.000482	0.003481	0.000464	0.600	0.570458
Right-Putamen	0.003466	0.000434	0.003472	0.000451	0.220	0.832807
Left-Accumbens-area	0.000437	0.000094	0.000417	0.000090	-1.149	0.294306
Right-Accumbens-area	0.000433	0.000053	0.000430	0.000051	-0.462	0.660093
Brain-Stem	0.014395	0.001062	0.014472	0.001101	1.403	0.210310

## A.2 Relative volumetric values for the ECT group

The volumetric values in the ROIs divided by the estimated total intracranial volume to account for different head sizes.

**Table A.2:** Relative mean value, standard deviation and p-value for the volumes in the ROIs for the ECT group. WM = White Matter, std = Standard Deviation

Areas	Scan 1 mean	Scan 1 std	Scan 4 mean	Scan 4 std	t-value	p-value
Left-Hippocampus	0.002611	0.000370	0.002684	0.000376	4.872	0.004587
Right-Hippocampus	0.002713	0.000347	0.002829	0.000343	14.314	0.000030
Left-Amygdala	0.001102	0.000207	0.001144	0.000215	2.459	0.057304
Right-Amygdala	0.001311	0.000172	0.001368	0.000185	6.715	0.001109
Left-Thalamus	0.004917	0.000597	0.004916	0.000567	-0.049	0.962538
Right-Thalamus	0.004709	0.000510	0.004786	0.000482	3.639	0.014912
Left-Caudate	0.002302	0.000295	0.002339	0.000285	1.487	0.197154
Right-Caudate	0.002375	0.000254	0.002389	0.000278	0.328	0.756416
Left-Cerebellum-WM	0.009119	0.001321	0.009484	0.001233	1.065	0.335517
Right-Cerebellum-WM	0.008649	0.001258	0.008940	0.001125	0.863	0.427434
Left-Cerebellum-Cortex	0.035200	0.003996	0.035176	0.003821	-0.120	0.909396
Right-Cerebellum-Cortex	0.035214	0.003814	0.035200	0.003760	-0.062	0.953226
Left-Pallidum	0.001194	0.000166	0.001237	0.000126	1.601	0.170228
Right-Pallidum	0.001265	0.000192	0.001322	0.000087	0.801	0.459490
Left-Putamen	0.003433	0.000464	0.003429	0.000564	-0.039	0.970462
Right-Putamen	0.003451	0.000376	0.003429	0.000516	-0.231	0.826533
Left-Accumbens-area	0.000408	0.000037	0.000389	0.000080	-0.622	0.561352
Right-Accumbens-area	0.000415	0.000062	0.000423	0.000070	0.577	0.589075
Brain-Stem	0.013879	0.001568	0.013966	0.001535	1.137	0.307077

### A.3 Relative volumetric values for the TMS group

The volumetric values in the ROIs divided by the estimated total intracranial volume to account for different head sizes.

**Table A.3:** Relative mean value, standard deviation and p-value for the volumes in the ROIs for the TMS group. WM = White Matter, std = Standard Deviation

Areas	Scan 1 mean	Scan 1 std	Scan 4 mean	Scan 4 std	t-value	p-value
Left-Hippocampus	0.002689	0.000384	0.002728	0.000377	1.793	0.116016
Right-Hippocampus	0.002730	0.000415	0.002782	0.000411	2.663	0.032317
Left-Amygdala	0.001136	0.000208	0.001136	0.000210	0.023	0.982267
Right-Amygdala	0.001323	0.000174	0.001314	0.000186	-0.559	0.593764
Left-Thalamus	0.004938	0.000513	0.004988	0.000496	1.218	0.262755
Right-Thalamus	0.004874	0.000458	0.004946	0.000423	2.409	0.046828
Left-Caudate	0.002450	0.000302	0.002475	0.000270	0.934	0.381197
Right-Caudate	0.002553	0.000257	0.002556	0.000250	0.105	0.919034
Left-Cerebellum-WM	0.009416	0.001393	0.009700	0.001771	1.462	0.187172
Right-Cerebellum-WM	0.009386	0.001528	0.009776	0.001892	2.162	0.067400
Left-Cerebellum-Cortex	0.036799	0.003188	0.037047	0.003484	0.629	0.549129
Right-Cerebellum-Cortex	0.037481	0.003392	0.037923	0.003579	0.581	0.579522
Left-Pallidum	0.001225	0.000147	0.001218	0.000162	-0.958	0.370200
Right-Pallidum	0.001252	0.000183	0.001256	0.000161	0.319	0.759273
Left-Putamen	0.003325	0.000432	0.003384	0.000427	1.433	0.195068
Right-Putamen	0.003460	0.000434	0.003510	0.000429	1.366	0.214325
Left-Accumbens-area	0.000381	0.000074	0.000377	0.000064	-0.246	0.812906
Right-Accumbens-area	0.000412	0.000050	0.000414	0.000057	0.395	0.704772
Brain-Stem	0.013832	0.000989	0.013949	0.000957	1.886	0.101289

# Appendix B

## Scripts

The scripts used in this thesis can be found in the GitHub repository via the link below. Both the FreeSurfer/BASIL analyses and the statistical analyses can be found in the repository.


<https://github.com/ingridkandersen/Master-Project>

# **Appendix C**

## **Poster for the MMIV conference**

The following poster was presented at the MMIV conference in December 2023.





# The effect of Electroconvulsive therapy (ECT) on brain perfusion and subcortical volume change in patients with major depression

Ingrid Kleive Andersen<sup>1</sup>, Frank Riemer<sup>2</sup>, Erling Andersen<sup>5</sup>, Hauke Bartsch<sup>2</sup>, Leila Marie Frid<sup>2</sup>, Ute Kessler<sup>3,4</sup>, Renate Gr uner<sup>1,2</sup>, Leif Olteidal<sup>2,3</sup>

<sup>1</sup> Department of Physics and Technology, University of Bergen, Norway. <sup>2</sup>Mohn Medical Imaging and Visualization centre (MMIV), Department of Radiology, Haukeland University Hospital, Norway. <sup>3</sup>Department of Clinical Medicine, University of Bergen. <sup>4</sup>Division of Psychiatry, Haukeland University Hospital, Norway. <sup>5</sup>Department of Clinical Engineering, Haukeland University Hospital, Norway

### Introduction

- Depression is a common and serious medical illness, and about one in six people will experience clinical depression in their life [1].
- Electroconvulsive therapy (ECT) is an effective treatment for many patients, particularly in patients with less effect from conventional treatment such as medication [2].
- ECT is performed by applying a series of brief electrical pulses via electrodes attached to the scalp, inducing a seizure [3].
- Volume increases have been shown in subcortical structures like the hippocampus after ECT treatment, e.g. [4].
- Brain perfusion, or Cerebral Blood Flow (CBF), is a measure of how much blood is delivered to the tissue from the vascular system.
- Arterial Spin Labelling (ASL) can be used to estimate CBF. With ASL, radio frequency pulses are used to label the inflowing blood to the brain, allowing to estimate cerebral blood flow in brain tissue through MRI, Figure 1. [5]
- Previous studies on ECT and perfusion mostly focus on perfusion indicating clinical outcome. [6]

### Methods

**Data:**

- Image data from 20 patients and 12 healthy controls were included in the analysis.
- Ten patients received ECT, and 10 patients received Transcranial Magnetic Stimulation (TMS).
- The patients participated in five MRI sessions: 1-7 days before, 1-2 hours after, 14 days after, 3-8 weeks after and 7-8 months after first treatment.
- The patients receive ECT treatment thrice a week until remission, or until reaching the upper limit of 18 treatments. [7]

**Processing:**

- "FreeSurfer" segmentation and volume quantification software was used to segment the anatomical image volumes (T1).
- A mask of the ROIs from the segmented image was used on the CBF.
- The anatomical analysis was as a mask on the CBF image to find the perfusion in the ROIs, Figure 2. Longitudinal analysis to estimate change in time were included.

### Goal and Hypothesis

- The goal of this project is to study possible perfusion and volumetric changes in selected brain structures as a response to ECT treatment.
- We hypothesize that changes in perfusion may precede volumetric changes, and that these findings may be correlated to the applied treatment regime (ECT).

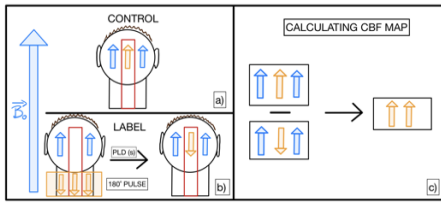


Figure 1: The working mechanism of Arterial Spin Labeling.  
a) The Control image. The blood-water in the brain has spin direction with  $B_0$   
b) The Labeled image. The blood-water in the neck is subject to a  $180^\circ$  pulse, inverting the spin. When the blood-water travels through the brain in the vascular system, it keeps spin direction against  $B_0$ . An image is taken after a set time, called the Post-Labeling Delay (PLD).  
c) Creating the CBF map. Subtracting the Labeled image from the control image removes the signal from the tissue, leaving only the signal from the blood-water

### Results and Conclusion

- A pipeline for automated analysis has been established. Preliminary results of CBF estimates in time in one healthy participant are shown in Figure 3.
- Analysis across participants will show how large variability there is across timepoints and if there is a difference in change in the participants receiving ECT treatment as compared to the participants receiving TMS.

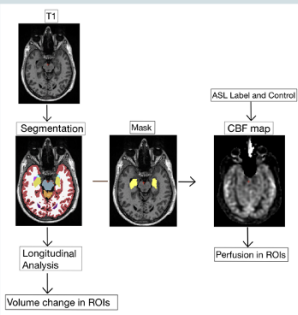


Figure 2: The pipeline used to process the data. FreeSurfers "recon-all" is used to segment the T1 image. The mask of the ROIs is then used on the CBF map to calculate CBF in the ROIs.

### References

- American Psychiatric Association, "What is Depression?".
- World Health Organization, Depressive disorder (depression).
- American Psychiatric Association, What is Electroconvulsive Therapy
- Olteidal L. et al., "Volume of the human Hippocampus and clinical response following electroconvulsive therapy".
- Clement, P., et al. (2022). "A Beginner's Guide to Arterial Spin Labeling (ASL) Image Processing". Frontiers in Radiology, 2.
- Leuner, A., M., et al. (2019). "Mechanisms of Antidepressant Response to Electroconvulsive Therapy Studied With Perfusion Magnetic Resonance Imaging". Biological Psychiatry, 85(6), 466-476.
- Frid, L. M., et al. (2023). "Neurobiological mechanisms of ECT and TMS treatment in Depression: study protocol of a multimodal magnetic resonance investigation". BMC Psychiatry, 23(1), 791.

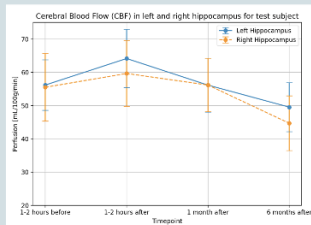


Figure 3: Cerebral Blood Flow in left and right hippocampus for one test subject

### Acknowledgments

The present study was funded by grants to L.O. and the Global ECT project, and the funding to R.G. from the Trond Mohn Foundation (#BFS2017TMT06). The authors want to thank all subjects participating in the study, and the MR technicians and research assistants who assisted in acquiring the data.








Figure C.1: The poster presented at the MMIV conference for the project in December 2023